UNIVERSITY OF CALIFORNIA SAN DIEGO

Seasonal changes in oceanographic conditions and mesoscale variability modulate cetacean predator-prey dynamics in the San Diego Trough

A Thesis submitted in partial satisfaction of the requirements
for the degree Master of Science

in

Marine Biology

by

Shelby Bloom

Committee in charge:

Professor Simone Baumann-Pickering, Chair
Professor John Hildebrand
Professor Dovi Kacev

2022

The Thesis of Shelby Bloom is approved, and it is acceptable in quality and form for publication on microfilm and electronically.

University of California San Diego

2022

DEDICATION

To my parents, David and Susan Bloom, who have sacrificed so much for me to get where I am today and have supported me throughout my journey, and to my sister, Tuesday Bloom, for cheering me on and always knowing I could do it.

TABLE OF CONTENTS

LIST OF FIGURES

LIST OF TABLES

LIST OF SUPPLEMENTAL VIDEOS

bloom_FSLE_FSLV_timeseries_movie.mov

ACKNOWLEDGEMENTS

I would first like to acknowledge my advisor, Simone Baumann-Pickering, for her support and mentorship through every step of this project. Without her, none of this would have been possible. Additionally, thank you to my committee members John Hildebrand and Dovi Kacev, for their helpful guidance.

I would also like acknowledge several post-docs, researchers, and fellow graduate students in the lab who were always willing to lend me a helping hand and share with me their knowledge, programming skills, and advice: Michaela Alksne, Ally Rice, Natalie Posdaljian, Vanessa Zobell, Annebelle Kok, Ashlyn Giddings, Morgan Ziegenhorn, Rebecca Cohen, and Catalina Aguilar. I'm particularly grateful to Michaela Alksne for allowing me to use her neural net for odontocete analysis and Ally Rice for detecting and classifying many of the mysticete calls.

I also wish to acknowledge everyone who has built and fixed equipment, coordinated instrument deployment and recovery, processed data, and so much more. Likewise, thank you to my collaborators Ana Širović and Joseph Warren.

Lastly, thank you to my parents and family for their unconditional love, support, advice, and encouragement.

Funding was provided by the Office of Naval Research, Marine Mammal and Biology Program, Dr. Michael Weise. This thesis, in full, is currently being prepared for submission for publication of the material. Bloom, Shelby; Baumann-Pickering, Simone; Rice, Ally; Širović, Ana; Warren, Joseph; Lankhorst, Matthias. The thesis author was the primary investigator and author of this material.

ABSTRACT OF THE THESIS

Seasonal changes in oceanographic conditions and mesoscale variability modulate cetacean predator-prey dynamics in the San Diego Trough

by

Shelby Bloom

Master of Science in Marine Biology

University of California San Diego, 2022

Professor Simone Baumann-Pickering, Chair

In marine ecosystems, cetaceans are top predators that mostly exploit low- to mid-trophic level organisms. The presence and type of behavior displayed by cetaceans within a habitat is thus strongly driven by the physical oceanographic conditions that modulate the local prey. However, our understanding of how physical oceanography shapes foraging resources for cetaceans is still lacking due to the difficulty of simultaneously and continuously collecting prey and cetacean presence data. This study used passive acoustic, active acoustic, and *in situ* physical oceanographic observations collected from moorings located within the San Diego Trough, along with satellite-derived and ocean general circulation model measurements, to characterize the

local ecosystem and generate generalized additive models to examine how physics influences the relationships between lower and higher trophic levels. Here, I show how seasonal changes in oceanography and mesoscale variability modulate prey availability and thus cetacean presence and behavior within the San Diego Trough. Specifically, I found that surface prey was modulated by changes in mesoscale activity, diel vertically migrating mesopelagic species were modulated by wind-driven upwelling and primary productivity, and krill in the mid-water column were modulated by wind-driven upwelling, salinity at ~300 m depth, and primary productivity. These relationships were then reflected in the cetacean models, where the presence and type of behavior displayed by a group of cetaceans was influenced either by both the presence of their prey and the physical oceanographic conditions that modulate their prey, or by just the physical oceanographic conditions that modulate their prey. These results describe the predator-prey dynamics of some of the cetaceans found within the San Diego Trough and may aid in developing more accurate spatially explicit management actions to better manage and conserve these species in similar ecosystems.

INTRODUCTION

In marine ecosystems, cetaceans are top-predators that depend on efficiently locating and tracking low- to mid-trophic level organisms to obtain energy and nutrients (Frederiksen et al. 2006, Gaichas et al. 2009, Young et al. 2015). This can be a difficult task, as the abundance and distribution of their foraging resources tend to fluctuate over large spatial and temporal scales with changes in primary and secondary productivity driven by oceanographic conditions (Nishimoto & Washburn 2002, Ressler et al. 2005, Guiet et al. 2022). As a result, the presence and type of behavior displayed by cetaceans within a habitat is strongly related to their prey's response to oceanographic conditions. To better understand cetacean predator-prey dynamics within a habitat, we need to determine how the local physical environment is modulating prey resources for cetaceans and examine how cetaceans are reacting to that. Investigation into these relationships is challenging due to the difficulty of continuously and simultaneously collecting distribution and abundance data of cetaceans and their prey. Recently, the coupling of active and passive acoustic sensors, along with physical and oceanographic techniques (i.e., *in situ,* satellite-derived, and ocean general circulation model measurements) have allowed researchers to overcome this challenge (Širović & Hildebrand 2011, Buchan et al. 2021).

In the Southern California Bight (SCB), a variety of cetacean species are found including mysticetes, beaked whales, and delphinids (Rice 1965, Širović et al. 2004, Barlow & Forney 2007, Roch et al. 2011, Soldevilla et al. 2011, Sumich & Show 2011, Baumann-Pickering et al. 2014, Douglas et al. 2014, Širović et al. 2015, Scales et al. 2017, Simonis et al. 2017). Predominant mysticetes in the SCB include blue (*Balaenoptera musculus*), humpback (*Megaptera novaeangliae)*, fin (*B. physalus*), and grey (*Eschrichtius robustus*) whales (Rice

1965, Širović et al. 2004, Barlow & Forney 2007, Sumich & Show 2011, Douglas et al. 2014, Širović et al. 2015, Scales et al. 2017). Blue and humpback whales occur seasonally within the SCB and primarily use this area for foraging (Širović et al. 2004, Barlow & Forney 2007, Douglas et al. 2014, Širović et al. 2015). Fin whales also primarily use the SCB for foraging but are present year-round (Širović et al. 2004, Barlow & Forney 2007, Douglas et al. 2014, Širović et al. 2015, Scales et al. 2017). Grey whales occur seasonally in the area as part of their migrational corridor between breeding and foraging grounds (Rice 1965, Sumich & Show 2011). Mysticetes primarily forage on krill in the mesopelagic or small pelagic fish at the sea surface (Širović et al. 2004, Barlow & Forney 2007, Širović et al. 2015, Scales et al. 2017). Predominant odontocete species within the SCB include common dolphins (*Delphinus delphis*), Pacific-white sided dolphins (*Lagenorhynchus obliquidens*), Risso's dolphins (*Grampus griseus*), and Cuvier's beaked whales (*Ziphius cavirostris*), all of which use the SCB as foraging grounds (Barlow & Forney 2007, Roch et al. 2011, Soldevilla et al. 2011, Baumann-Pickering et al. 2014, Simonis et al. 2017). Delphinids primarily forage on surface prey and diel vertically migrating mesopelagic species (Roch et al. 2011, Soldevilla et al. 2011, Simonis et al. 2017), while beaked whales primarily forage on mesopelagic or bathypelagic cephalopods (Tepsich et al. 2014).

All cetacean species produce sound to communicate, odontocetes additionally echolocate to navigate and detect their prey (Au & Hastings 2008). Two call types commonly produced by blue whales are B calls and D calls. B calls are believed to be associated with reproduction (Oleson et al. 2007), while D calls are believed to be associated with feeding (McDonald et al. 2001, Oleson et al. 2007, Lewis et al. 2018). Humpback whales produce song and non-song calls (Payne & McVay 1971, Stimpert et al. 2011, Vu et al. 2012, Herman 2017). Song calls have been recorded only from males and are regarded as breeding displays but have been

recorded on both feeding and breeding grounds, while non-song calls are social calls that have been shown to be associated with group foraging (Stimpert et al. 2011, Vu et al. 2012, Herman 2017). Fin whales produce two types of low-frequency calls termed 20 Hz and 40 Hz calls (Širović et al. 2012, Širović et al. 2015, Romagosa et al. 2021). Studies suggest that 20 Hz calls serve a reproductive function, while 40 Hz calls serve a food-associated function (Širović et al. 2012, Romagosa et al. 2021). The predominant call produced by migrating grey whales are M3 calls (Crane & Lashkari 1996). Odontocetes produce echolocation clicks to detect, characterize, and localize prey, and these clicks are often species-specific (Soldevilla et al. 2008, Roch et al. 2011, Baumann-Pickering et al. 2013).

The San Diego Trough is a bathyal basin within the SCB that is located off San Diego, California (Eckman & Thistle 1991). Its long axis is oriented approximately northwest-southeast (Eckman & Thistle 1991). Diverse physical processes influence the Trough, including the California Undercurrent, the California Countercurrent, equatorward wind-driven upwelling, and mesoscale features such as eddies, fronts, and filaments (Hickey 1979, 1992, Checkley & Barth 2009). Both the California Undercurrent and California Countercurrent are poleward flowing currents (Hickey 1979, 1992, Checkley & Barth 2009). The California Undercurrent is a subsurface (100-300 m) current that brings warmer, saltier equatorial or southern waters to the Trough, while the California Countercurrent is a surface current that carries a mixture of Pacific subarctic water from the California Current and Eastern North Pacific Central water (Hickey 1979, 1992, Checkley & Barth 2009).

In this study, I use passive and active acoustic recordings and *in situ* water measurements from oceanographic moorings located within the San Diego Trough, along with satellite-derived and ocean general circulation model environmental data, to show how local physical

oceanography shapes cetacean predator-prey dynamics within the San Diego Trough. I first examine the *in situ*, satellite-derived, and ocean general circulation model environmental variables to characterize and describe the local oceanographic conditions. Then, I use the active acoustic recordings and environmental data to generate generalized additive models (GAMs) to examine the relationships between the prey communities relevant to cetaceans found foraging in the area and the physical environment. Finally, I use the passive acoustic recordings, active acoustic recordings, and environmental data to generate GAMs to examine the relationships between presence and type of behavior displayed by cetaceans in the area and oceanographic and prey conditions. With a better understanding of cetacean predator-prey dynamics within the San Diego Trough, it may be possible to manage and conserve these species in similar ecosystems more effectively by generating more accurate spatially explicit management actions.

METHODS

i. Study Region and Mooring Data Collection

Between August 2016 and January 2018, oceanographic moorings were deployed on three occasions at a site (Site T) within the San Diego Trough (Fig. 1, Table 1). Passive acoustic recordings, acoustic backscatter data, and *in situ* water measurements were collected during each deployment using a high-frequency acoustic recording package (HARP) suspended approximately 25 m above the seafloor (Wiggins et al. 2006), a Simrad EK80 Wide Band Autonomous Transceiver (WBAT, Kongsberg Maritime, Lynnwood, WA) located ~300 m from the water surface facing upward, and an autonomous Sea-Bird SBE 37-SMP MicroCAT (Sea-Bird Electronics, Bellevue, WA) located ~300 m from the water surface, respectively (Fig. S1). For deployment 1, two moorings were deployed approximately 1 km apart, with one mooring equipped with the WBAT and ~300 m MicroCAT, and the other with the HARP (Table 1). For deployments 2 and 3, a single mooring equipped with all 3 instruments was deployed (Table 1). Temporal coverage among instrument data and between deployments varied because of battery life, data storage capacity, and servicing efforts (Table 1).

For each deployment, HARPs were programmed to record continuously at a sampling rate of 200 kHz with a 16-bit amplitude resolution, providing an effective recording bandwidth from 0.01 to 100 kHz. Hydrophones were lab calibrated and a transfer function was applied during data analysis. This allowed for the detection of both mysticete low-frequency calls and odontocete high-frequency echolocation clicks. WBATs were outfitted with a 70 kHz split-beam transducer with nominal 18° opening angle to examine pelagic fish and a 200 kHz split-beam transducer with nominal 7° opening angle to examine zooplankton. Both transducers operated in continuous-wave mode and were programmed to collect a set number of active as well as passive

pings at a duty cycle (Table S1). Echosounders were calibrated using the standard sphere method (Demer et al. 2015) and the resulting parameters from calibration were used during processing. MicroCATs were programmed to obtain samples every minute for deployment 1, and every 6 minutes for deployments 2 and 3.

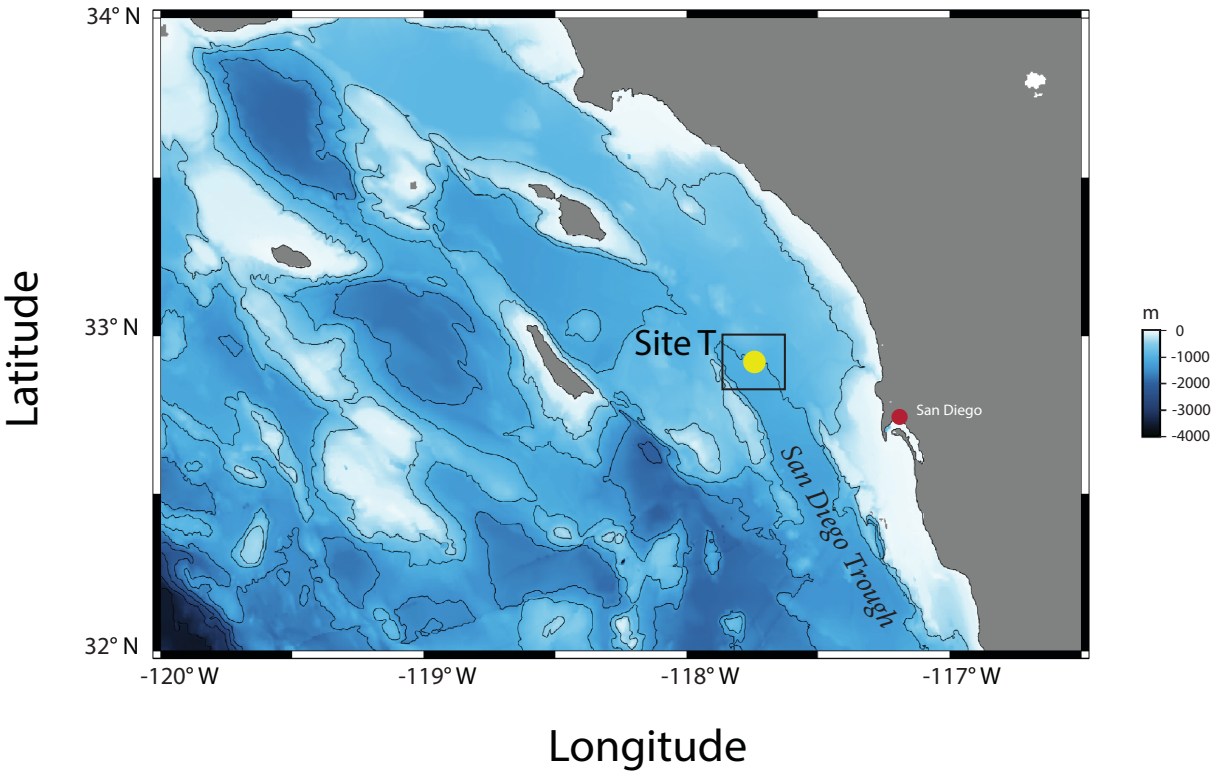

Figure 1: Map of study site. Map showing the latitude-longitude location of the study site (Site T) denoted as the yellow dot. Location of the site was averaged among deployments. The black box represents the 20x20 km area around Site T that was used to average environmental variables over. Blue color bar represents water depths. Black lines indicated 500 m contours. Grey denotes land masses.

Table 1: Summary of mooring locations, depths, instrumentation, and instrumentation recording periods for each deployment

Deployment	Mooring	Location	Depth (m)	HARP Recording Dates	WBAT Recording Dates	~300 m MicroCAT Recording Dates
1	SOCAL_T_01_A	32° 53.210' N, 117° 33.370' W	827	---	8/18/2016-12/14/2016	8/18/2016-12/14/2016
	SOCAL_T_01_B	32° 53.210' N, 117° 36.586' W	900	9/29/2016-12/15/2016	---	---
2	SOCAL_T_02	32° 53.212' N, 117° 33.362' W	825	3/5/2017-7/6/2017	3/15/2017-7/6/2017	3/5/2017-7/6/2017
3	SOCAL_T_03	32° 53.199' N, 117° 33.496' W	814	7/8/2017-1/17/2018	7/8/2017-11/14/2017	7/8/2017-1/17/2018

ii. Passive Acoustic Data Analysis

Odontocetes

Echolocation clicks of Cuvier's beaked whales, Risso's dolphins, common dolphins, and Pacific white-sided dolphins were identified using a combination of automated detection and classification methods, and manual verification. First, an automated detection algorithm described by Roch et al. (2011) was implemented on the full bandwidth passive acoustic recordings to detect and return all acoustic signals that resembled odontocete echolocation clicks. These signals were then passed through an unsupervised clustering algorithm that identified and clustered consistent signal types together within every five-minute bin of every deployment (Frasier et al. 2017). Once clustered, a supervised deep neural network trained to classify bin-

level average clicks corresponding to Cuvier's beaked whales, Risso's dolphins, common dolphins, and both click types (A and B) associated with Pacific white-sided dolphins (PWS A and PWS B) (Soldevilla et al. 2008), was used to label the five-minute bin-level clusters (Frasier 2021, Alksne et al. in prep). The network's architecture consisted of four 512-node fully connected layers with 50% dropout between layers and a maximum of 15 epochs allowed (Alksne et al. in prep). It was trained using five-minute bin-level clusters of the five click types from two recording sites off Southern California and one site located in Quinault Canyon within the Olympic Coast National Marine Sanctuary off the coast of Oregon (Alksne et al. in prep). Signals that were assigned labels from the neural network were manually reviewed in the software DetEdit (Solsona-Berga et al. 2020), a MATLAB-based graphical user interface that allows users to visualize inter-click-intervals (ICIs), long-term spectral averages (LTSAs) (Wiggins et al. 2006), received levels, and spectrums of clicks classified by the neural network. False positives and clicks with a peak-to-peak received level below 120 dB re 1 μPa were removed, ensuring that only reliable detections remained (Solsona-Berga et al. 2020).

Clicks corresponding to Cuvier's beaked whales were not detected during the recording period. Clicks corresponding to Risso's dolphins and the two click types associated with Pacific-white sided dolphins were binned into 1-minute intervals, and the number of 1-minute intervals with any number of echolocation clicks present was used to define presence of those click types. I will refer to these as click positive minutes. Similar to Risso's and Pacific white-sided dolphins, common dolphin echolocation clicks were initially binned into click positive minutes. However, common dolphins were present every day in the recording period, so I decided to focus on their predator-prey relationships rather than just presence. As such, I defined presence of clicks corresponding to common dolphins in each 1-minute interval based on a minimum number of

720 click detections. This threshold was motivated by the mode of observed inter-click intervals of 56ms (Fig. S2), signifying that an actively foraging common dolphin would produce 1080 clicks in a minute. My definition then means that a common dolphin had to be actively foraging for two thirds of that 1-minute interval for it to be counted as presence. I will call this foraging positive minutes. Daily summed counts of click positive minutes and foraging positive minutes were used to measure presence of respective click types.

Mysticetes

All mysticete calls were identified using decimated acoustic data, allowing for more effective scanning and detection of low-frequency calls. Blue, fin, and gray whale calls were analyzed using data that was decimated by a factor of 100, for an effective acoustic bandwidth up to 1 kHz, while humpback whale calls were analyzed using data that was decimated by a factor of 20, for an effective acoustic bandwidth up to 5 kHz.

Individual blue whale D calls were automatically detected using a modified version of the generalized power law detector (Helble et al. 2012). All detections were manually verified by a trained analyst (Ally Rice) and false positives were removed. Daily summed counts of calls were used to measure blue whale D call presence.

Individual blue whale B calls were automatically detected using spectrogram correlation (Mellinger & Clark 2000, Širović et al. 2015). To account for variation in detector performance due to seasonal and interannual shifts in B call frequency (McDonald et al. 2009) and seasonal changes in call abundance (Širović 2016), deployment-specific kernels and thresholds were utilized (Table S2 and S3). Overall, detector precision and recall were above 70% for each

deployment (Table S2). Daily summed counts of calls were used to measure blue whale B call presence.

Fin whale 20 Hz calls were automatically detcted using an energy detection method that uses the difference in acoustic energy between signal at 22 Hz and noise (Širović et al. 2004, Nieukirk et al. 2012). Noise was calculated as the average energy between 10 and 34 Hz (Nieukirk et al. 2012, Širović et al. 2015). Daily averages of the resulting ratio termed 'fin whale acoustic index', were calculated and used to measure fin whale 20 Hz call presence.

Fin whale 40 Hz calls were manually detected by a trained analyst (Ally Rice) using *Triton*, custom MATLAB (Mathworks, Natick, MA) software, to visually scan 1-hour LTSAs created using a 5-sec time average and a 1-Hz frequency resolution . Individual calls were verified using 60-sec spectograms (2000-point fast Fourier transform (FFT) length, 90% overlap). The LTSA frequency was set to display between 1 and 300 Hz and the spectogram window was set to display between 1 and 200 Hz. The hourly presence of fin whale 40 Hz calls was logged and summed daily to measure fin whale 40 Hz call presence.

Gray whale M3 calls were manually detected using *Triton* to visually scan 1-hour LTSAs created using a 5-sec time average and a 1-Hz frequency resolution. Individual calls were verified using 60-sec spectograms (2000-point FFT length, 90% overlap). The LTSA frequency was set to display between 1 and 350 Hz and the spectogram window was set to display between 1 and 200 Hz. No gray whale M3 calls were detected during the recording period.

Humpback whale calls (there was no discrimination between song and non-song call types) were manually detected using *Triton* to visually scan 1-hour LTSAs created using a 5-sec time average and a 10-Hz frequency resolution. Calls were verified using 30-sec spectograms (1000-point FFT length, 90% overlap). The LTSA frequency was set to display between 1 and

5000 Hz and the spectogram window was set to display between 1 and 2000 Hz. Humpback whale calls were grouped into encounters, and the start and end time of each encounter was recorded. An encounter ended when a call was followed by at least 30 minutes of recording with no other humpback whale calls. Start and end times of encounters were converted into hourly presence, and daily sums of hourly presence were used to measure humpback whale acoustic presence.

iii. Active Acoustic Data Analysis

All WBAT-echosounder data was processed using Echoview software version 9.0 (Echoview Software Pty Ltd, Hobart, Myriax). Raw data was calibrated using parameters obtained from the echosounder calibrations, as well as temperature and salinity measurements collected by the ~300 m MicroCAT. These measurements were used to calculate and adjust the sound speed via the Chen & Millero equation (Chen & Millero 1977). Once calibrated, maximum-strength single beam echograms were calculated for each frequency, and background noise and low-level signals were removed. This was established by applying the background noise removal operator in Echoview and setting an echo strength threshold of -70 dB. Surface and bottom analysis boundaries were then generated to exclude the top 5 m and bottom 13 m of the water column. Positioning of the surface boundary line was selected to account for swaying of the upward-facing active acoustic sensor on the mooring line and time periods of stronger wave action at the sea surface, while positioning of the bottom boundary line was selected to account for any effects that resulted from the measurements being in the vicinity of the sensor. Next, cells of 1-minute intervals by 50-m depths between the sea surface and the sensor at depth were generated, resulting in depth bins of 5-50 m, 50-100 m, 100-150 m, 150-200 m, 200-250 m,

and 250-277 m due to the analysis boundaries. Backscatter strength was calculated for each cell as the Nautical Area Scattering Coefficient (NASC), and daily median NASC values of each depth bin for the 70 kHz and 200 kHz frequencies were used to provide an estimate of fish and zooplankton presence, respectively (Maclennan et al. 2002).

iv. Environmental Data Analysis

Eleven environmental variables were obtained from moored MicroCATS and open-access internet databases of satellite-derived and ocean general circulation model measurements. *In situ* temperature (C°) and salinity (PSU) data at ~300 m were derived from samples collected by the moored Sea-Bird SBE 37-SMP MicroCATs using SeaBirdDataProcessing-Win32 software (Sea-Bird Electronics, Bellevue, WA) and averaged daily. Satellite-derived and ocean general circulation model environmental data were accessed through ERDDAP (Environmental Research Division's Data Access Program, http://coastwatch.pfeg.noaa.gov/erddap/index.html), HYCOM (Hybrid Coordinate Ocean Model, https://www.hycom.org) and AVISO+ (Archiving, Validation and Interpretation of Satellite Oceanographic Data, https://www.aviso.altimetry.fr/en/) internet databases. Datasets were selected based on their spatial and temporal coverage and resolution (Table 2). The environmental variables obtained from these databases included sea surface height, sea surface temperature, sea surface salinity, chlorophyll A concentration, backwards-in-time finite-size Lyapunov exponents (FSLEs), associated finite-size Lyapunov vector (FSLV) orientations, wind-driven upwelling index, mixed layer thickness derived from isopycnal layers, and mixed layer thickness derived from temperature (Table 2). Upwelling indices were computed from Ekman transport data using the Bakun Upwelling Index calculation (Bakun 1973, 1975). All satellite-derived and ocean general

circulation model environmental variables were averaged daily over an area as close as possible to 20 km around Site T to account for the spatial range of cetacean detections (Fig. 1). Daily standard deviations were also obtained for FSLEs and FSLV orientations.

Table 2: Summary of data source, data set, and resolution (spatial and temporal) for satellite-derived and ocean general circulation model environmental variables.

Environmental Variable	Data Source	Data Set	Spatial Resolution	Temporal Resolution
Sea Surface Height (m)	HYCOM	GOFS 3.0 Global Analysis GLBa0.08 expt_91.2	1/12 degree	Daily
Sea Surface Temperature (°C)	ERDDAP	SST, NOAA POES AVHRR, LAC, 0.0125 degrees, West US, Day and Night, 2004-present (1 Day Composite), degree F, Lon+/-180	1/80 degree	Daily
Sea Surface Salinity (PSU)	HYCOM	GOFS 3.0 Global Analysis GLBu0.08 expt_91.2	1/12 degree	Daily
Chlorophyll A Concentration (mg/m^3)	ERDDAP	Chlorophyll, NOAA VIIRS, Science Quality, Global, Level 3, 2012-present, Daily	1/28 degree	Daily
Finite-size Lyapunov Exponents (per day)	AVISO+	DT FSLE	1/25 degree	Daily
Finite-size Lyapunov Vector Orientations (°)	AVISO+	DT FSLE	1/25 degree	Daily
Upwelling Index	Derived from ERDDAP	FNMOC Ekman Transports, 360x180, 6-hourly, Lon+/-180	1 degree	6 hours
Mixed Layer Thickness (m) via isopycnal layers	HYCOM	GOFS 3.0 Global Analysis GLBa0.08 expt_91.2	1/12 degree	Daily
Mixed layer thickness (m) via temperature	HYCOM	GOFS 3.0 Global Analysis GLBa0.08 expt_91.2	1/12 degree	Daily

FSLEs and their associated FSLV orientations are used to detect and characterize Lagrangian coherent structures (d'Ovidio et al. 2004, Titaud et al. 2011, Peacock & Haller 2013). When calculated backwards-in-time, these structures represent areas of convergence between water parcels, such as those around the outside of eddies or between fronts (d'Ovidio et al. 2004, Titaud et al. 2011, Peacock & Haller 2013). FSLEs measure the intensity of the convergence zone (d'Ovidio et al. 2004), with more negative values representing more intense and stronger convergence (Fig. S3C). FSLV orientations describe the orientation of the normalized eigenvectors of the Lagrangian coherent structures (Titaud et al. 2011), where the variable theta max is given as the anticlockwise orientation in degrees with respect to East (Fig. S3A). They can be used to interpret the orientation of the FSLE filaments, since it is expected that the FSLV is oriented normal to the FSLE filament tangent (Fig. S3B and Fig. S3C). By averaging over the 20 x 20 km area around Site T, I used FSLEs as a measure of mesoscale activity and FSLV orientations as a measure of the orientation of FSLE filaments in the area.

iv. Characterization of Local Physical Oceanography

To characterize the physical oceanography at Site T, I generated weekly averaged time-series plots of the environmental variables, along with weekly averaged contour plots of salinity, temperature, and water origin. The contour plots were generated using unpublished methods by Matthias Lankhorst, Scripps Institution of Oceanography, and data obtained from the California State Estimation – Short-Term State Estimation (CASE-STSE) solutions database (Ocean State Estimation at Scripps, http://www.ecco.ucsd.edu/case_stse_results1.html). Water origin was determined by corresponding temperature and salinity values from the CASE-STSE database to a given water mass described using a North-South index. The index was constructed using

climatological data obtained off Southern California that generated enveloping lines of potential temperature and practical salinity values that varied exactly between -1 and +1 for northern and southern origin, respectively. For a given temperature-salinity value, the N-S index was computed by interpolating between the two lines from -1 to +1. A negative number, or Northern index, indicates that the water mass is comprised of cold, fresh water from sub-polar regions and a positive number, or Southern index, indicates that the water mass is comprised of warm, salty water from sub-tropical regions. Additionally, daily maps of FSLE and FSLV orientations were plotted to examine mesoscale features throughout the period of observation.

v. Generalized Additive Models

GAMs were constructed using the R software package *mgcv* (Wood 2006). Since the focus of this study was on cetacean predator-prey dynamics in relation to physical oceanography, all models were generated over the time span when there was simultaneous collection of passive acoustic recordings, acoustic backscatter data, and *in situ* water measurements. This time frame was from 2016 September 29 – 2017 November 14. For the prey models, prey presence was the response variable and the covariates were the environmental variables. For the cetacean models, cetacean presence was the response variable and the covariates were the environmental and prey presence variables. To account for temporal autocorrelation, response and predictor variables for each model were averaged over time bins motivated by auto-correlation function (ACF) plots of the response variable generated using the *acf* function in R. Bins encompassing days without full effort of passive acoustic recordings, acoustic backscatter data, or *in situ* water measurements were removed from analysis. Additionally, if there was missing satellite-derived or ocean general circulation model environmental data after binning, then these were interpolated using the

na_interpolation function in R (Moritz & Bartz-Beielstein 2017). If needed, data transformations of the response and predictor variables were implemented based on their histograms. Each model was fit using either a Gaussian distribution with an identity link function or a Tweedie distribution with a log link function, depending on the distribution of the response variable observations. For all models, predictor variables were modeled as smooth additive terms using the default basis thin plate regression spline and smoothing parameters were selected using the "Restricted Maximum Likelihood" method (REML) with a four-knot basis to reduce overfitting. To determine the optimal set of explanatory variables, all models used a forward model selection process due to the limited number of observations compared to predictor variables. The forward selection process began with fitting single variable models for every predictor variable and generating a subset of the original predictor variables that contained only those that were statistically significant ($p < 0.05$). These significant predictor variables were then examined for collinearity using a correlation matrix of the original set of predictor variables and multicollinearity using variance inflation factors (VIF) derived from the set of significant predictor variables. Of the variables that had collinearity (correlation coefficient > +/- 0.6) or multicollinearity (VIF > 3), one of the variables would be removed based on their Akaike information criterion (AIC) (Zuur et al. 2009). This final subset of predictor variables was used for the rest of the model fitting process. Next, a single variable null model was generated using the predictor variable with the lowest AIC value from the final subset. A series of models were then fit in a stepwise fashion, where one new predictor variable from the final subset was added to the null model and the models were compared for fit based on AIC. The best model was selected based on AIC. All models were evaluated using the *gam.check* function in R.

RESULTS

i. Physical Oceanography

Water at the sea surface exhibited a seasonal cycle in temperature, with warmer waters occurring in the summer and fall months, while salinity of the water had no clear seasonal pattern but appeared to fluctuate with changes in water origin (Fig. 2). Water at ~300 m depth exhibited a seasonal cycle in both temperature and salinity, with warmer, more saline waters observed during the summer and fall months (Fig. 2).

Seasonal cycles were observed for many of the physical processes, including mixed layer thickness, wind-driven upwelling indices, sea surface height, and mesoscale activity (Fig. 2). Mixed layer thickness was greatest during winter, with a peak in thickness occurring in January (Fig. 2). Sea surface height was greatest beginning in late summer and continuing through early winter (Fig. 2). Upwelling dominated over the late spring to fall months (Fig. 2, Fig. 3B), corresponding with low sea surface height in this near coastal region, and was replaced with mesoscale activities, visible in the FSLE measurements, in the other time periods (Fig. 2, Fig. 3A). Orientations of the FSLE filaments fluctuated throughout the period of observation and had no clear seasonal pattern.

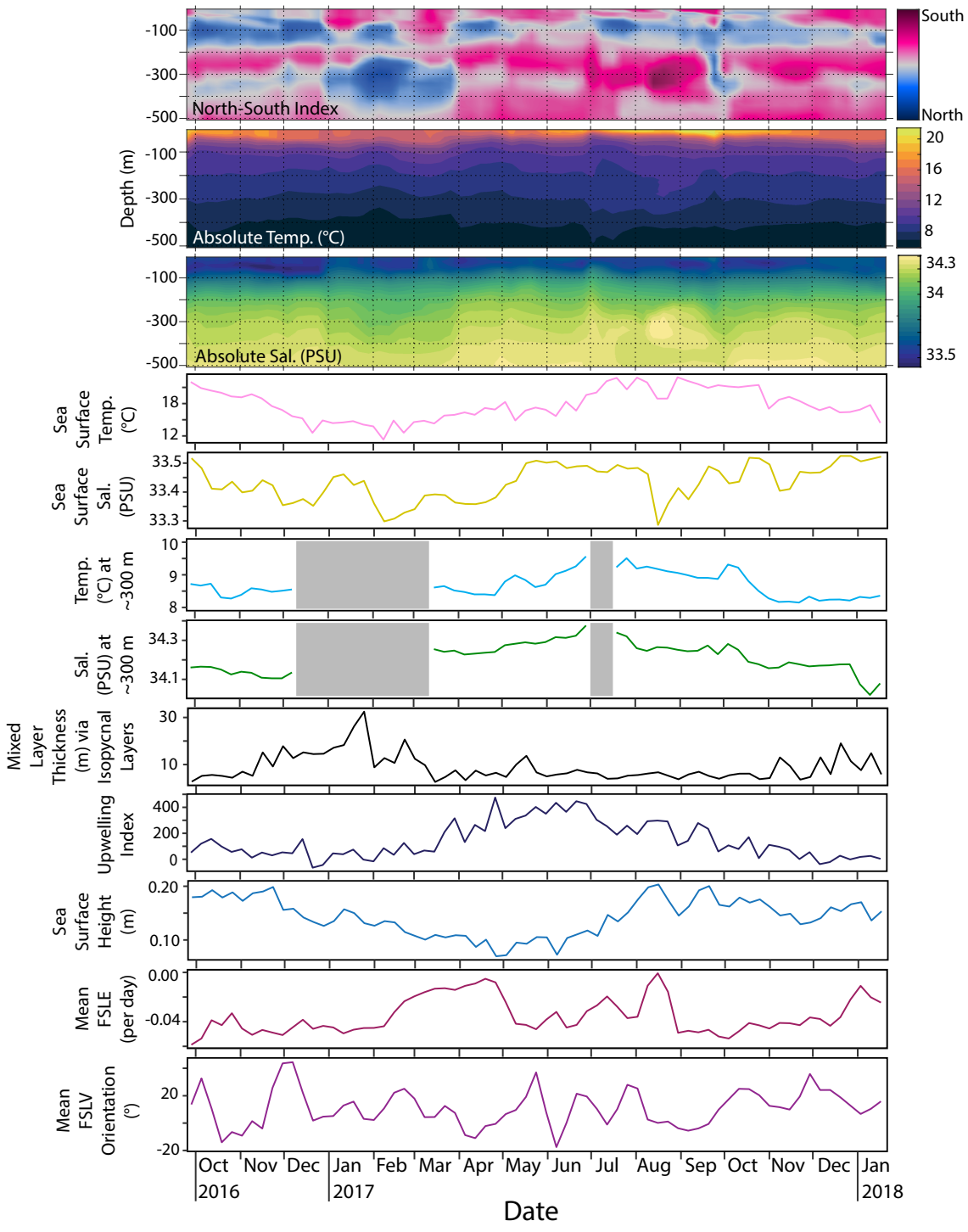

Figure 2: Physical oceanography at study site. Contour plots with weekly averages of North-South index, absolute temperature (°C), absolute salinity (PSU) over 500 m depths (modeled data), and below weekly averaged time series of temperature (°C) and salinity (PSU) at sea surface, temperature (°C) and salinity (PSU) at 300 m depth, mixed layer thickness (m), upwelling index, sea surface height (m), FSLE (per day) and FSLV orientation (°). Gray shading represents data gap.

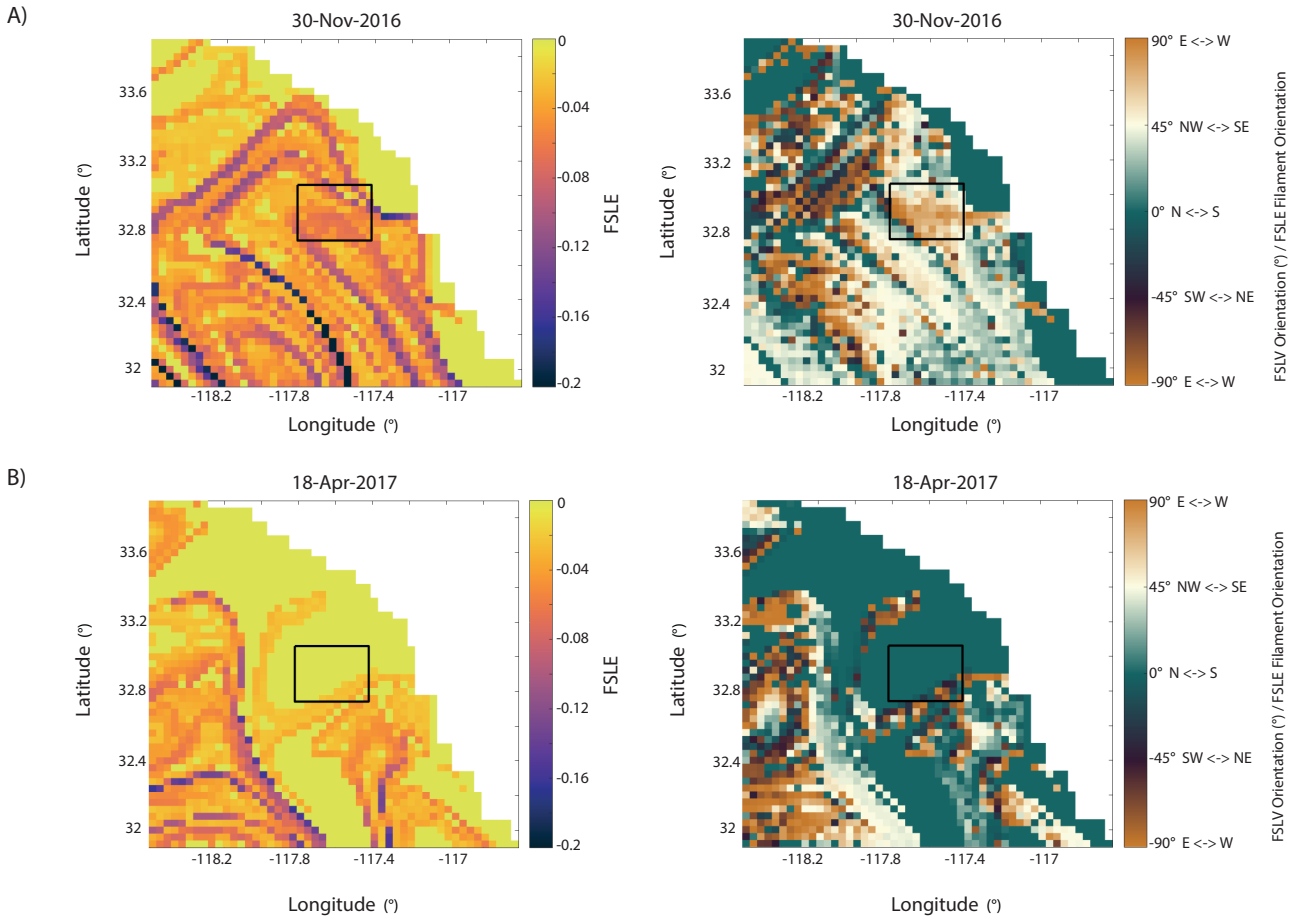

Figure 3: Plots of FSLE intensity (left) and FSLV orientation (right) during (A) mesoscale activity and (B) upwelling dominated time periods. Black box represents a 20x20 km area around Site T over which environmental variables were averaged. FSLE: darker colors represent more negative FSLE values, hence stronger convergence zone. FSLV: color bar represents the FSLV orientation in degrees, with FSLE filament orientation given as compass orientation.

ii. Prey Community

When examining the prey community at Site T, I focused on characterizing communities that would be relevant to the cetacean species found foraging in the area, namely mysticetes and delphinids. As such, we selected 70 kHz NASC measurements between 5-50 m to represent pelagic fish near the surface, 70 kHz NASC measurements between 100-150 m to represent diel vertically migrating prey, and 200 kHz NASC measurements between 200-250 m to represent

mid-water krill. Measurements of near surface krill were out of reach of the acoustic instrument based on placement of the upward-oriented transducer at 300 m.

Daily medians of 70 kHz NASC between 5-50 m were averaged over 6 days to account for autocorrelation (Table 3). Data was log-transformed due to the distribution of observations being positively skewed. Model was fit using a Gaussian distribution with an identity link function (Table 3). Overall, there was a total of 50 observations included in the model (Table 3). Mean FSLEs was the only predictor variable found to be significant (Fig. 4A, Table 3). The relationship between 70 kHz NASC between 5-50 m and mean FSLEs was negative, where an increase in 70 kHz NASC between 5-50 m was predicted when there was less mesoscale activity in the area (Fig. 4A). The final model explained 26.1% of the deviance and had an overall good fit (Table 3, Fig. S4).

Daily medians of 70 kHz NASC between 100-150 m were averaged over 6 days to account for autocorrelation (Table 3). Data was log-transformed due to the distribution of observations being positively skewed. Model was fit using a Gaussian distribution with an identity link function (Table 3). Overall, there was a total of 50 observations included in the model (Table 3). The model with the best predictive power incorporated log chlorophyll A concentration and upwelling index (Fig. 4B, Table 3). The relationship between 70 kHz NASC between 100-150 m and log chlorophyll A concentration was generally positive and exhibited wide confidence intervals due to low sample size at higher values of chlorophyll concentration (Fig. 3B). 70 kHz NASC between 100-150 m had a dome-shaped relationship with upwelling indices, with a favorable range seen around 200 (Fig. 3B). The final model explained 38% of the deviance and had an overall good fit (Table 3, Fig. S5).

Table 3. Summary of statistical outputs of best generalized additive models (GAMs) explaining 70 kHz nautical area scattering coefficient (NASC) over two depth bins and presence of four call types over three cetacean species. Formulas for best models are shown below table. All predictor variables were modeled as smooth additive terms using the default basis thin plate regression spline (bs = "ts'). Smoothing parameters were selected using the "Restricted Maximum Likelihood" method (REML) and the number of basis functions was set to 4. Models were fit using either a Gaussian distribution with identity link function or a Tweedie distribution with log link function, depending on the distribution of the response variable observations. The Tweedie variance power p value is provided in the formulas below when applicable. Predictor variables are shown with abbreviation and measurement depth in meters. The categorical P-value significance for each predictor variable is given as ***<0.001; **<0.01; *<0.05. Abbreviations: mean_fsle - mean finite size Lyaponuv exponent (per day); log.chlor - log chlorophyll a concentration (mg/mi^3); UpwellingIndex - upwelling indices; mean_theta - mean finite size Lyaponuv vector orientation (°); mean_temp300 - mean water temperature (°C) at ~300 m depth; mean_mlt_pycno - mean mixed layer thickness (m) derived via isopycnal layers; mean_ssh - mean sea surface height (m); X200.NASC.250.277 - 200 kHz NASC between 250-277 m; std_theta - standard deviation of finite size Lyaponuv vector orientation (°); X70.NASC.100.150 - 70 kHz NASC between 100-150 m; X200.NASC.200.250 - 200 kHz NASC between 200-250 m.

Response Variable	Bin Size (in days)	n	Est	Std. Error	t value	P-value	R^2 adj	Dev. exp. (%)	F	P-value	F	P-value	F	P-value	F	P-value	F	P-value
Log 70 kHz NASC 5-50 m	6	50	3.05	0.10	30.42	<2e-16 ***	0.23	26.1	6.12	s(mean_fsle) 0.0026 **								
Log 70 kHz NASC 100-150 m	6	50	0.74	0.05	15.23	<2e-16 ***	0.32	38	5.50	s(log.chlor) 0.0040 **	3.25	s(UpwellingIndex) 0.0472 **						
Common Dolphin Foraging Positive Minutes	6	50	37.39	2.11	17.71	<2e-16 ***	0.32	37	6.83	s(UpwellingIndex) 0.0032 **	3.52	s(mean_theta) 0.0401 *						
Blue Whale D Calls	5	62	0.42	0.24	1.71	0.0929	0.51	75.2	6.22	s(UpwellingIndex) 0.0158 *	6.98	s(mean_temp300) 0.0108 *	18.15	s(mean_mlt_pycno) 8.42e-05 ***	9.31	s(mean_ssh) 0.0001 ***	13.01	s(X200.NASC.250.277) 9.83e-5 ***	10.08	s(std_theta) 0.0025 **
Blue Whale B Calls	8	38	2.75	0.26	10.66	5.58e-12 ***	0.09	57.9	9.31	s(mean_ssh) 1.19e-5 ***	16.49	s(X70.NASC.100.150) 0.0003 ***	6.26	s(X200.NASC.200.250) 0.0176 *	5.78	s(mean_theta) 0.0222 *		
Fin Whale 40 Hz Calls	2	158	-1.28	0.14	-9.12	4.68e-16 ***	0.32	28.8	4.89	s(mean_fsle) 0.0019 **	11.12	s(mean_ssh) 0.0011 **	4.66	s(mean_temp300) 0.0090 **	16.49	s(X70.NASC.100.150) 0.0003 ***		

log(70 kHz NASC 5-50 m) ~ s(mean_fsle, k = 4) - Gaussian; identity link
log(70 kHz NASC 100-150 m) ~ s(log.chlor, k = 4) + s(UpwellingIndex, k = 4) - Gaussian; identity link
Common Dolphin Foraging Positive Minutes ~ s(UpwellingIndex, k = 4) + s(mean_fsle, k = 4) - Gaussian; identity link
Blue Whale D Calls ~ s(UpwellingIndex, k = 4) + s(mean_temp300, k = 4) + s(mean_mlt_pycno, k = 4) + s(mean_ssh, k = 4) + s(X200.NASC.250.277, k = 4) + s(std_theta, k = 4) - Tweedie p = 1.628; log link
Blue Whale B Calls ~ s(mean_ssh, k = 4) + s(X70.NASC.100.150, k = 4) + s(X200.NASC.200.250, k = 4) + s(mean_theta, k = 4) - Tweedie p = 1.713; log link
FIn Whale 40 Hz Calls ~ s(mean_fsle, k = 4) + s(mean_ssh, k = 4) + s(mean_temp300, k = 4) + s(X70. NASC.100.150, k = 4) - Tweedie p = 1.103 ; log link

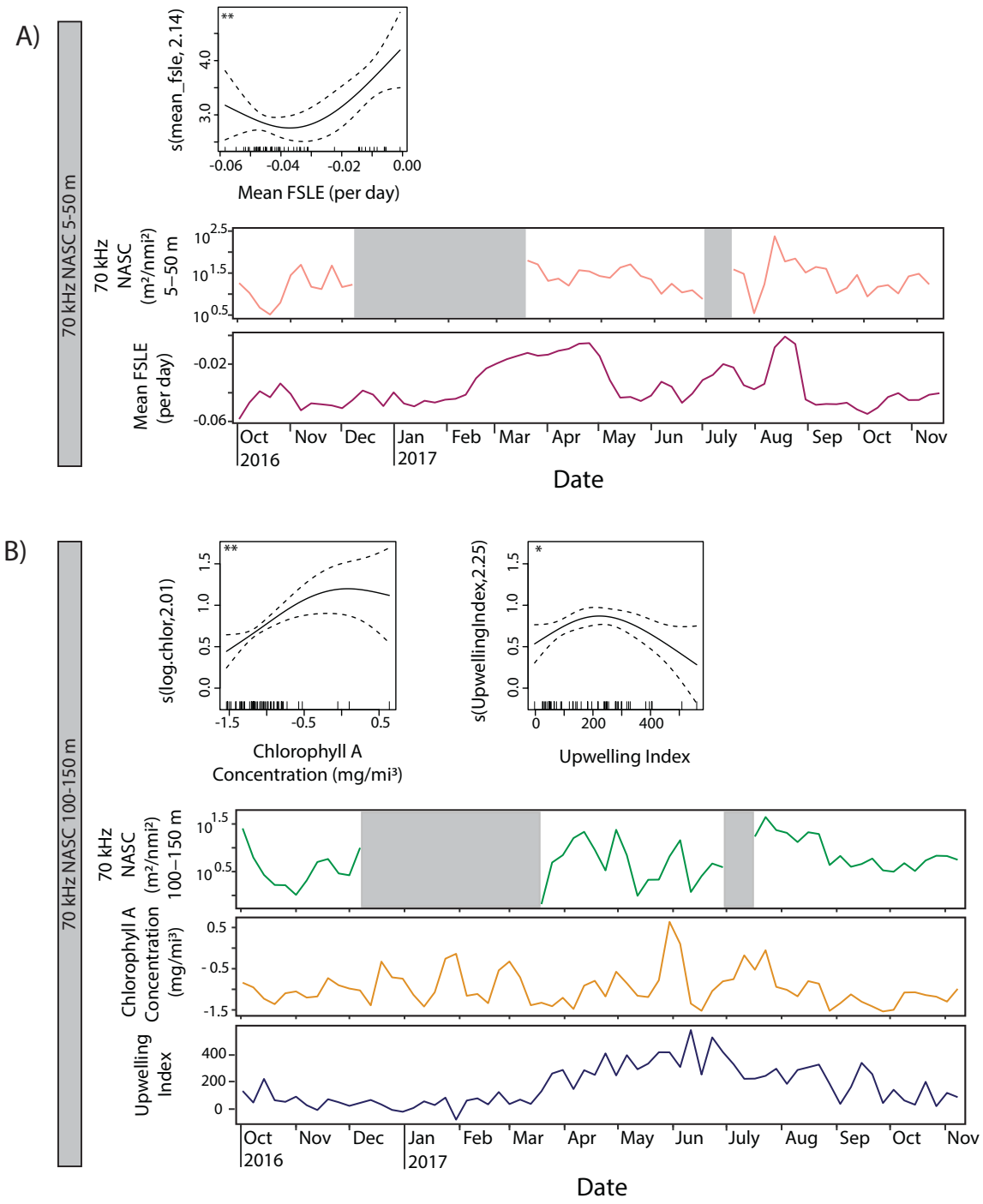

Figure 4: Generalized additive model outputs and time series for (A) 70 kHz NASC between 5-50m and (B) 70 kHz NASC between 100-150m. The model spline per predictor variable is displayed for each model with y-axis label indicating effective degrees of freedom. The *P*-level per variable is given as ***<0.001; **<0.01; and *<0.05. The corresponding binned time series of the best model response and predictor variables are presented. Gray shading represents no effort time periods.

The temporal autocorrelation of daily medians of 200 kHz NASC between 200-250 m were too large to bin and still retain enough observations to generate a predictive GAM. However, it was observed that 200 kHz NASC between 200-250 m was generally positively correlated with water salinity at ~300 m, upwelling index, and chlorophyll A concentrations (Table 4, Fig. S6) when looking at the various correlation matrices generated for the different cetacean models and binning (detailed further below).

Table 3: Summary of variables significantly (+/- 0.06) correlated with 200 kHz NASC between 200-250 m. Correlation coefficients are provided for each bin size, based upon cetacean models. Abbreviations: Dd foraging – common dolphin foraging positive minutes, Bm B – blue whale B calls, Bm D – blue whale D calls, Bp 40 Hz – fin whale 40 Hz calls.

Significant Variables	6 Day Bin (Dd foraging)	8 Day Bin (Bm B)	5 Day Bin (Bm D)	2 Day Bin (Bp 40 Hz)
Mean Chlorophyll A Concentration (mg/m^3)	--	0.60	--	--
Upwelling Index	0.62	0.67	0.61	--
Mean Salinity (PSU) at ~300 m	0.61	0.63	0.63	--

ii. Cetaceans

Blue whale B and D calls had a strong seasonal cycling, with B calls occurring predominantly during the fall and winter months and D calls occurring predominantly during the summer and early fall months (Fig. 5). When blue whale B and D calls were both present, an inverse relationship was observed, where if there was an increase in D calls there was a decrease in B calls, and vice versa (Fig. 5). Fin whale 20 Hz calls occurred all throughout the recording effort but had a peak in acoustic index during the late fall and winter months (Fig. 5). Fin whale 40 Hz calls fluctuated throughout the recording effort with no clear seasonal pattern (Fig. 5). Humpbacks exhibited a strong seasonal acoustic presence, with most detections beginning in late fall and continuing through early spring (Fig. 5). Common dolphin clicks occurred throughout the recording period with little to no fluctuation in presence (Fig. 5). Common dolphin foraging periods occurred throughout the recording effort, with a slight drop in presence during the summer months (Fig. 5). Pacific white-sided dolphin type A (PWS A) clicks were rarely detected and only during the late spring to early fall months (Fig. 5). Pacific white-sided dolphin type B (PWS B) clicks occurred predominantly during the fall to winter months (Fig. 5). Risso's dolphin clicks fluctuated throughout the year with no clear seasonal pattern (Fig. 5). Overall, blue, fin and humpback whales were the most frequently detected mysticetes, while common dolphins were the most frequently detected odontocetes. Due to the large temporal autocorrelation of fin whale 20 Hz calls as well as humpback whale calls, these were excluded from further analysis. Additionally, sparse presence of other delphinid species prohibited modeling effort for these signal occurrences. In the end, common dolphin foraging positive minutes, blue whale B and D calls, and fin whale 40 Hz hourly presence were modeled.

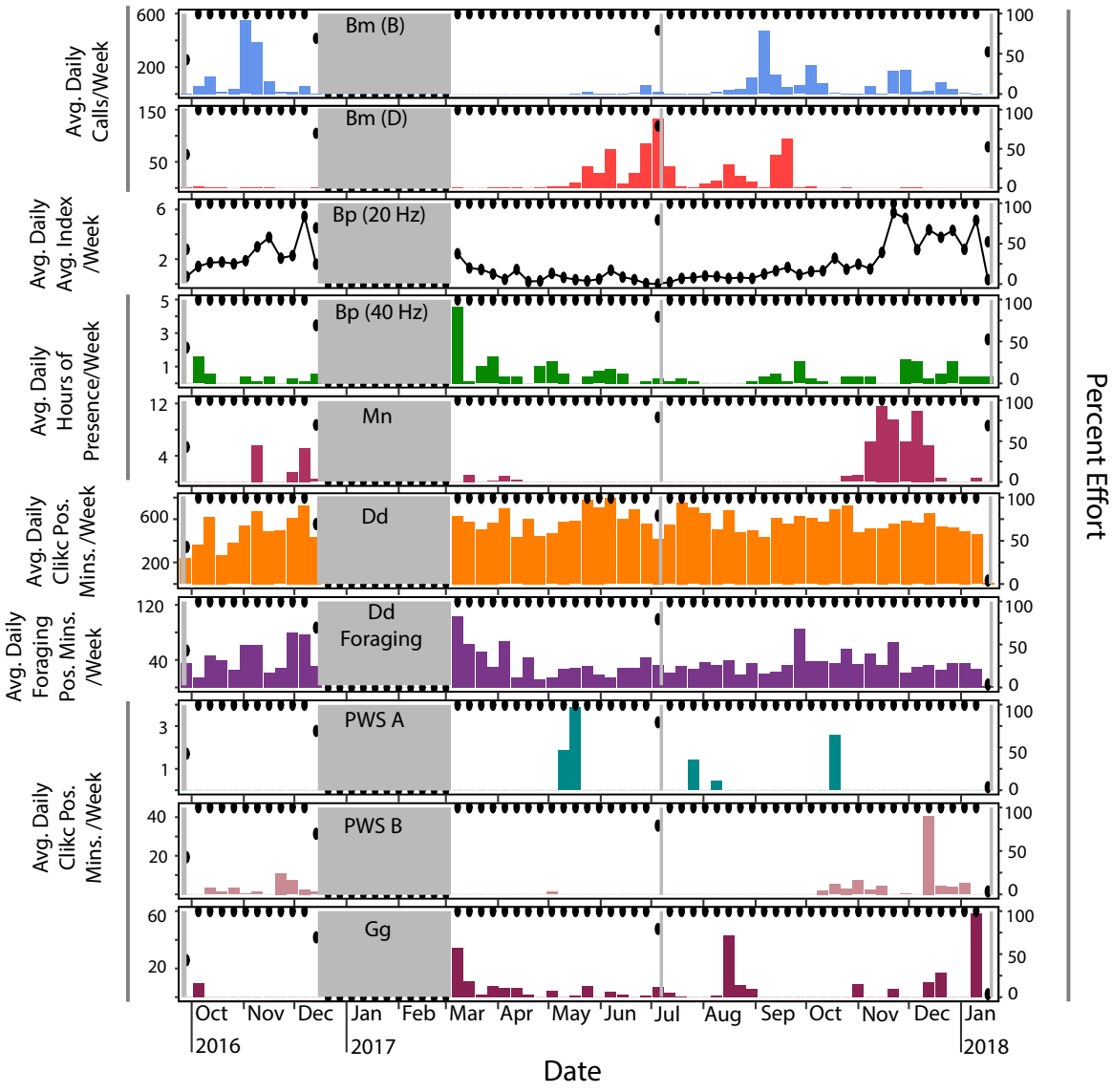

Figure 5: Averaged weekly presence of all cetacean species detected in the passive acoustic recordings. Percentage of detection effort per day with black dots. Time periods without recordings shaded gray. Abbreviations: Bm (B) – blue whale B calls, Bm (D) – blue whale D calls, Bp (20 Hz) – fin whale 20 Hz index, Bp (40 Hz) – fin whale 40 Hz calls, Mn – humpback song and non-song calls, Dd – common dolphins, Dd Foraging – common dolphin foraging, PWS A – Pacific white-sided dolphin type A, PWS B – Pacific white-sided dolphin type B, Gg – Risso's dolphin.

Daily sums of common dolphin foraging positive minutes were averaged over 6 days to account for autocorrelation (Table 3). Model was fit using a Gaussian distribution with an

identity link function (Table 3). Overall, there was a total of 50 observations included in the model (Table 3). The most important predictors were upwelling index and mean FSLV orientation (Fig. 6, Table 3). Foraging positive minutes had a negative relationship with upwelling index, and a generally positive relationship with mean FSLV orientation (Fig. 6). The final model explained 37% of the deviance and had an overall good fit (Table 3, Fig. S7).

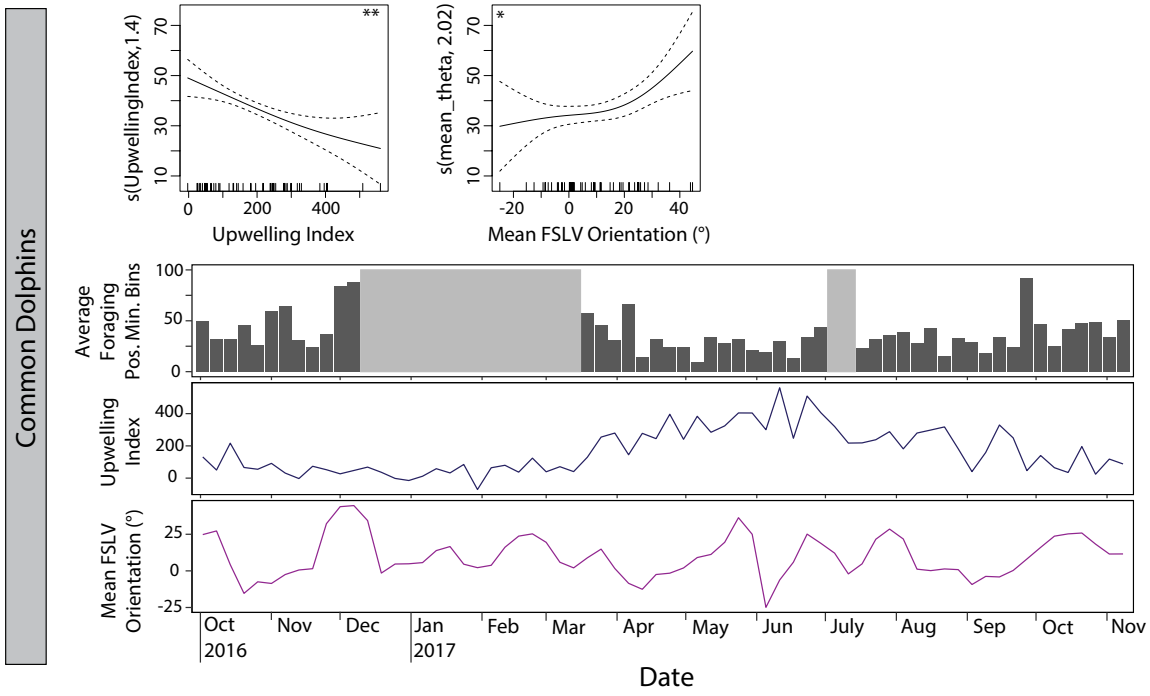

Figure 6: Generalized additive model outputs and time series of common dolphin foraging positive minutes. The model spline per predictor variable is displayed for each model with y-axis label indicating effective degrees of freedom. The *P*-level per variable is given as ***<0.001; **<0.01; and *<0.05. The corresponding binned time series of the best model response and predictor variables are presented. Gray shading represents no effort time periods.

Blue whale D daily counts of calls were averaged over 5 days (Table 3). Model was fit using a Tweedie distribution with a log link function (Table 3). Overall, there was a total of 62

observations included in the model (Table 3). The most important predictors were upwelling index, water temperature at ~300 m, mixed layer thickness derived from isopycnal layers, sea surface height, 200 kHz NASC between 250-277 m, and standard deviation of FSLV orientation (Fig. 7A, Table 3). Blue whale D call acoustic presence increased with increasing upwelling index, water temperature at ~300 m, and 200 kHz NASC between 250-277 m (Fig. 7A). It decreased with increasing mixed layer thickness derived from isopycnal layers and standard deviation of FSLV orientation (Fig. 7A). There was a strong increase in abundance with sea surface height above 0.16 m (Fig. 7A). The relationship was less clear with sea surface heights below 0.16 m (Fig. 7A). The final model explained 75.2% of the deviance and had an overall good fit (Table 3, Fig. S8).

Daily counts of blue whale B calls were averaged over 8 days (Table 3). A best model was fit using a Tweedie distribution with a log link function (Table 3). Overall, there was a total of 38 observations included in the model (Table 3). The most important predictors were sea surface height, 70 kHz NASC between 100-150 m, 200 kHz NASC between 200-250 m, and mean FSLV orientation (Fig. 7B, Table 3). Blue whale B call acoustic presence increased with increasing 200 kHz NASC between 200-250 m and decreased with increasing 70 kHz NASC between 100-150 m and mean FSLV orientation (Fig. 7B). A positive relationship between B call count and sea surface height is suggested, which is leveling off around 0.16 m (Fig. 7B). The final model explained 57.9% of the deviance and had an overall good fit (Table 3, Fig. S9).

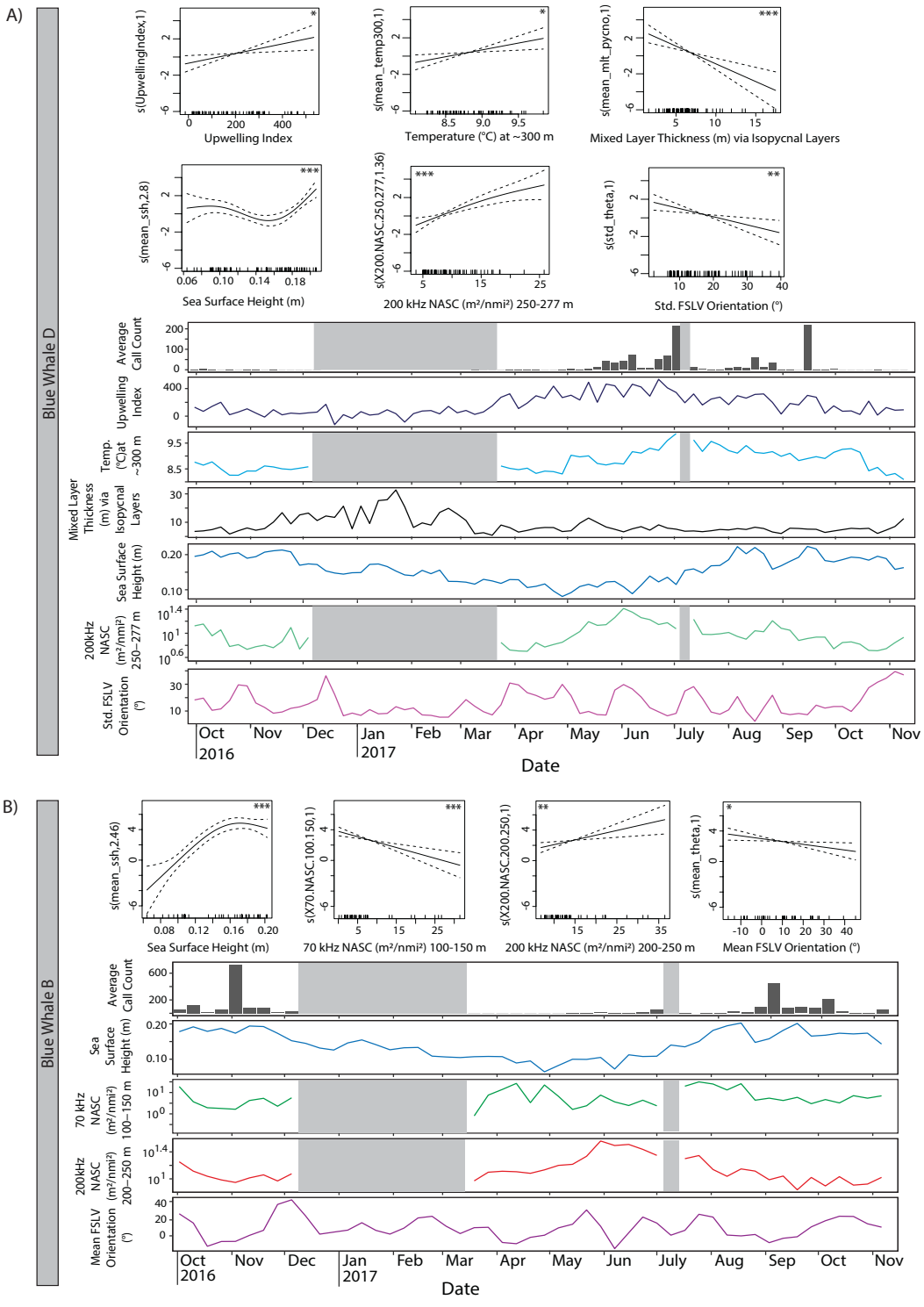

Figure 7: Generalized additive model outputs and time series for (A) blue whale D calls and (B) blue whale B calls. The model spline per predictor variable is displayed for each model with y-axis label indicating effective degrees of freedom. The *P*-level per variable is given as ***<0.001; **<0.01; and *<0.05. The corresponding binned time series of the best model response and predictor variables are presented. Gray shading represents no effort time periods.

Daily hourly presence of fin whale 40 Hz calls was averaged over 2 days (Table 3). Model was fit using a Tweedie distribution with a log link function (Table 3). Overall, there was a total of 158 observations included in the model (Table 3). The model with the best predictive power incorporated mean FSLEs, sea surface height, water temperature at ~300 m, and 70 kHz NASC between 100-150 m (Fig. 8, Table 3). Fin whale 40 Hz calls had a negative relationship with sea surface height and water temperature at ~300 m, and a positive relationship with 70 kHz NASC between 100-150 m (Fig. 8). There was a general decrease in presence with a decrease in FSLEs, with a favorable range of mean FSLEs seen around -0.02 (Fig. 8). The final model explained 28.8% of the deviance, but had a relatively poor fit (Table 3, Fig. S10).

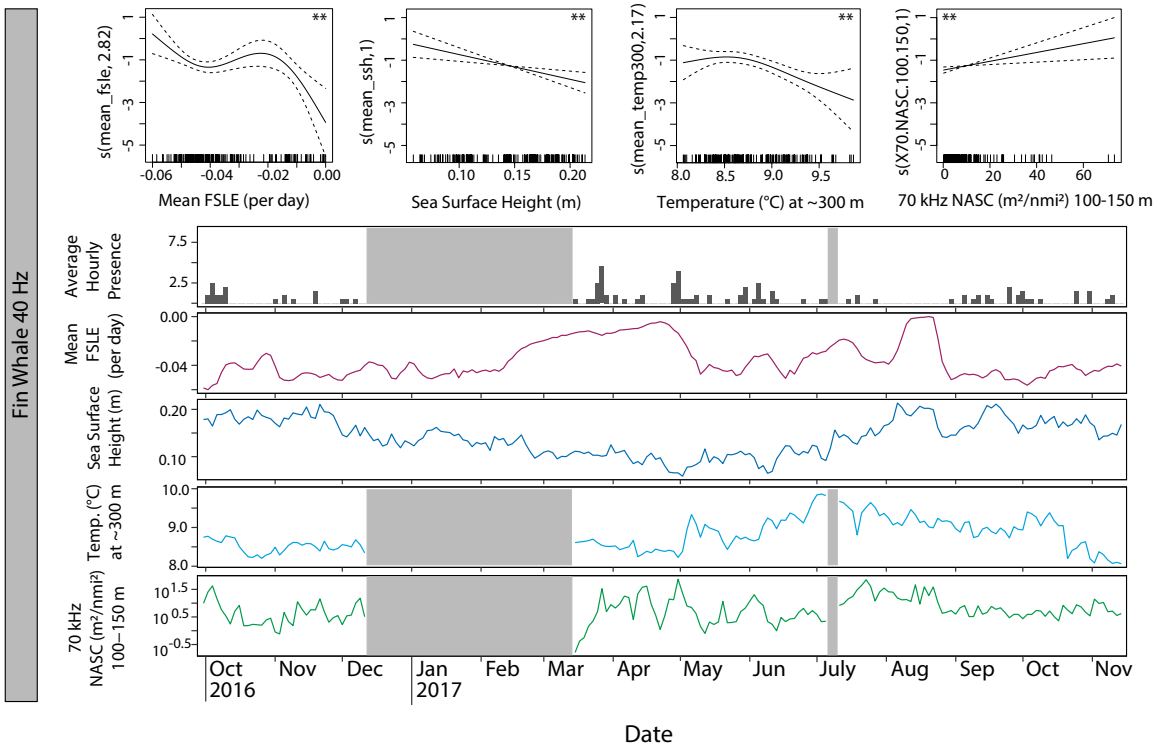

Figure 8: Generalized additive model outputs and time series of fin whale 40 Hz calls. The model spline per predictor variable is displayed for each model with y-axis label indicating effective degrees of freedom. The *P*-level per variable is given as ***<0.001; **<0.01; and *<0.05. The corresponding binned time series of the best model response and predictor variables are presented. Gray shading represents no effort time periods.

DISCUSSION

In this study, I have used passive acoustics, active acoustics, *in situ* water measurements, and satellite-derived and ocean general circulation model environmental variables, to investigate cetacean predator-prey dynamics within the San Diego Trough. Examination into the local physical oceanography showed that many of the physical processes at Site T had a seasonal cycle. A dynamic relationship between wind-driven upwelling and mesoscale features was also observed, where the seasonal cycle of coastal wind-driven upwelling appeared to push mesoscale features out of the broader San Diego Trough region. Examination into the relationships between oceanographic conditions and the prey community showed that surface prey was modulated by changes in mesoscale activity, diel vertically migrating mesopelagic species were modulated by wind-driven upwelling and primary productivity, and krill in the mid-water column were modulated by wind-driven upwelling, salinity at ~300 m, and primary productivity. Cetaceans detected at Site T included blue whales, fin whales, humpbacks whales, common dolphins, Risso's dolphins, and Pacific white-sided dolphins. The most frequently detected mysticetes were blue, fin and humpback whales, while the most frequently detected odontocete species was common dolphins. Investigation into the relationships between the oceanographic conditions, prey community, and cetacean species (specifically common dolphins, blue whales, and fin whales) showed that seasonal changes in the oceanography, mesoscale variability, and prey presence, modulated the presence and type of behavior displayed by these cetaceans.

i. Prey Community

The resulting model for 70 kHz NASC between 5-50 m highlights the influence mesoscale features had on surface prey. The negative relationship between 70 kHz NASC at 5-

50 m and mean FSLEs illustrate that the presence of surface prey increased during time periods with little to no mesoscale activity. This may appear contradictory at first, as many studies have suggested that mesoscale features enhance biological production in the ocean (Falkowski et al. 1991, Oschlies & Garçon 1998, Siegel et al. 1999). However, in nearshore upwelling systems like the San Diego Trough, mesoscale features and horizontal stirring have been shown to suppress production by transporting nutrients from the nearshore environment to the open ocean (Rossi et al. 2009, Gruber et al. 2011). Thus, prey at the surface may benefit from relaxation periods in horizontal stirring because nutrient-rich waters are not being transported out of the area and therefore primary productivity increases.

For 70 kHz NASC between 100-150 m, the modeled relationships highlight the influences wind-driven upwelling and chlorophyll A concentrations had on diel vertically migrating mesopelagic species. The positive relationship between 70 kHz NASC at 100-150 m and chlorophyll A concentrations illustrate that the presence of diel vertically migrating species increased with increasing primary productivity, which is consistent with many studies (Davison et al. 2013, Irigoien et al. 2014). The dome-shaped relationship between upwelling and presence of mesopelagic species is consistent with findings from Ruzicka et. al. (2016) who found similar relationships across a variety of trophic levels in the Northern California Current ecosystem. Essentially, increases in upwelling intensity increase productivity by exporting needed nutrients to the surface, but it becomes detrimental at very high upwelling intensities by physically exporting nutrients out of the area too quickly for phytoplankton to exploit, and by physically exporting phytoplankton out of the area too quickly for higher trophic levels to exploit (Ruzicka et al. 2016). The combination of these two physical exports therefore inhibit the presence of

mesopelagic species by taking away their prey, and by taking away needed nutrients for their prey.

The correlations for 200 kHz NASC between 200-250 m demonstrate the influences that chlorophyll A concentrations, upwelling indices, and salinity at ~300 m had on krill in the mid-water column. The positive relationship with chlorophyll A concentrations show that the presence of krill increased with increasing primary productivity, which is consistent with other studies (Croll et al. 2005, Ressler et al. 2005, Cimino et al. 2020). The positive relationship with upwelling indices may be the result of krill benefiting from seasonal upwelling events that bring cold-nutrient rich waters to the surface that phytoplankton exploit, which in turn increase primary productivity for the krill to exploit (Croll et al. 2005, Ressler et al. 2005, Cimino et al. 2020). When looking at the time series of the local physical oceanography, we see that salinity at ~300 m had a seasonal cycle during the summer and fall months, which coincided with the onset of seasonal upwelling (Fig. 2). Thus, the cause of a positive relationship between salinity at ~300 m and the presence of krill at depth could just be an indirect relationship that is caused by the concurrent increase in upwelling. However, increased salinity at ~300 m was also observed when there were more Southern waters in the area, presumably from the California Undercurrent (Fig. 2). Therefore, the positive relationship with salinity at ~300 m could also be from the transport of Southern waters into the area that are carrying phytoplankton that the krill then exploit (Bialonski et al. 2016).

ii. Cetaceans

Common dolphin foraging positive minutes had significant relationships with upwelling and mean FSLV orientations, which suggest that the dolphins reacted to how these

oceanographic processes modulated their foraging resources. As seen from the prey models, wind-driven upwelling had a detrimental effect on the presence of diel vertically migrating mesopelagic species at higher upwelling intensities. Since this is one of the prey communities that common dolphins forage on (Simonis et al. 2017), it is consistent to see a negative relationship between common dolphin foraging activity and upwelling. The positive relationship between common dolphin foraging activity and mean FSLV orientations may be the result of prey aggregations within the San Diego Trough due to the orientation of FSLE filaments aligning with the northwest-southeast orientation of the Trough. Bathyal features that generate high sea floor relief such as troughs are known to attract top predators including cetaceans by creating areas of entrapment of phytoplankton and zooplankton (Hui 1979, Selzer & Payne 1988). Additionally, studies have shown that phytoplankton and the environments in which they are embedded in converge to that of FSLE structures (d'Ovidio et al. 2010, Lehahn et al. 2018). With that, I interpret that when the orientation of FSLE filaments align with the San Diego Trough, the Trough acts as a funnel and entraps primary productivity, zooplankton and nekton which then increase the presence of foraging resources for common dolphins.

The relationships found for blue whale D calls illustrate how blue whale foraging activity was influenced by their prey and the oceanographic conditions that modulated their prey. As seen in the model, blue whale D calls increased with increasing backscatter strength of 200 kHz NASC between 250-277 m (i.e., krill in the mid water-column), which is consistent with other studies (Buchan et al. 2021). The positive relationship between D calls and upwelling index is consistent with earlier findings that the presence of krill in the mid-water column increased with increasing upwelling, suggesting that blue whale foraging activity was also influenced by this physical process due to how it modulated its prey. Temperature at ~300 m was highly correlated

with salinity at ~300 m (correlation coefficient of 0.79) for this model, therefore I interpret the significance of temperature at ~300 m to be associated with how krill was modulated by salinity at ~300 m. The seasonal cycle of sea surface height was closely correlated with upwelling index (correlation coefficient of -0.54), thus I suggest that the significance of sea surface height is associated with how krill was modulated by upwelling. Similarly, the negative relationship between mixed layer thickness via isopycnal layers and D calls also seems to be the result of how krill was modulated by upwelling. As seen in the time series of the local physical oceanography, mixed layer thickness via isopycnal layers was greatest during the winter months, which contradicted the onset of seasonal upwelling (Fig. 2). The negative relationship observed with standard deviation in FSLV orientation indicates that blue whale foraging activity increased when there were less dramatic changes in FSLE filament orientations. This may benefit blue whale foraging by allowing for aggregations in prey.

For blue whale B calls, the relationships found to be significant illustrate how the whales may be switching behavior from foraging to presumed breeding based on the conditions that modulated their prey. The positive relationship with sea surface height may be the result of krill presence decreasing with decreasing upwelling, as seen in the analysis of krill in the mid-water column and oceanographic conditions. Higher sea surface heights were observed when there was less upwelling and in turn less krill (Fig. 2). Thus, the blue whales are likely switching their behavior from foraging (D calls) to presumed breeding (B calls) during lower krill presence in the area. The negative relationship between 70 kHz NASC between 100-150 m (i.e., diel vertically mesopelagic species) and the positive relationship between 200 kHz NASC between 200-250 m (i.e., krill in the mid-water column) with blue whale B calls seem to be significant in terms that it describes the underlying, related ecosystem processes. Essentially, we are having a

waning of krill and thus blue whales are reducing their feeding activity and likely switching to mating (B calls), but there may still remain enough krill in the area intermittently so that the whales still positively react to that. I interpret the negative relationship between FSLV orientations and blue whale B calls in the same manner as above, where the San Diego Trough acts as a funnel and entraps primary productivity when the orientation of FSLE filaments align with the orientation of the Trough. However, instead of benefiting from this entrapment, blue whale B calls decrease when this happens because blue whales are switching to foraging due to aggregations of their prey.

The positive relationship between 70 kHz NASC between 100-150 m (i.e. diel vertically migrating mesopelagic species) illustrate that foraging activity of fin whales was directly influenced by the backscatter strength of their potential fish prey. However, the relationships between the 40 Hz calls and the physical oceanographic conditions that came out of the model as significant were more difficult to interpret when compared to blue whales. It is probably the result of these animals being generalists that feed on both krill and small pelagic species (Jory et al. 2021) and frequenting the SCB region year round (Širović et al. 2015). The negative relationship with sea surface height contradicts the environmental conditions found to increase the presence of mesopelagic species, but they do align with the physical conditions shown to increase the presence of krill. The seasonal cycle of sea surface height was closely correlated with upwelling index (correlation coefficient of -0.47), thus I suggest that the significance of sea surface height is associated with how krill was modulated by upwelling. The relationship between 40 Hz calls and temperature at ~300 m is a representative measure of general ecosystem seasonality, while the relationship with FSLE intensity could be indicative of their preferred prey to associate with strong mesoscale features (Scales et al. 2017, Scales et al. 2018).

CONCLUSION AND FUTURE DIRECTIONS

This study provided one of the first comprehensive analyses of cetacean predator-prey dynamics using the coupling of passive and active acoustic sensors. As seen from the results, when coupled with oceanographic measurements, this approach can reveal dynamic and complex relationships by providing a whole-picture view of the ecosystem.

The prey models presented here indicate that seasonal cycles of oceanographic conditions and physical forcing seem to be key processes in modulating foraging resources for cetaceans in the San Diego Trough. As seen, the presence of pelagic fish near the surface and mid-water krill increased with oceanographic conditions associated with seasonal upwelling dominated periods, while the presence of diel vertically migrating species increased with oceanographic conditions associated with seasonal mesoscale dominated periods. Additionally, the cetacean models demonstrated that the presence and behavior of cetaceans inhabiting the Trough are influenced by oceanographic conditions that modulate their prey. Common dolphin foraging periods increased during mesoscale dominated oceanographic conditions which correspond with increased presence of diel vertically migrating species. Blue whales exhibited foraging activity during upwelling dominated conditions which corresponded with increased presence of mid-water krill, and switched to presumed breeding activity during mesoscale dominated conditions which corresponded with the waning of krill. Fin whale foraging activity was more complex to model, and is most likely the result of these animals being generalists and frequenting the SCB year-round.

To build a more holistic understanding of cetacean predator-prey dynamics within the Trough, future research would benefit from the continued collection of passive and active acoustic data at this site. This would add to the already existing modeling efforts and allow for

one to obtain even better predictive models. Additionally, future efforts could also explore other modeling techniques such as generalized additive mixed models with generalized estimating equations or Bayesian techniques, which could potentially grasp more underlying relationships by already accounting for temporal autocorrelation. There are also other ways of looking at the active acoustic data, and future research might be able to gain something looking at dB differencing and amplifying the organismic group behind the backscatter data.

The ability to predict species-specific cetacean occurrence in the San Diego Trough by examining cetacean predator-prey dynamics is especially pertinent to effectively manage and conserve cetacean species in similar ecosystems. This is because we have a better understanding of the oceanographic and prey conditions that influence their presence and behavior within a habitat and can therefore make more accurate spatially explicit management actions.

Acknowledgements

This thesis, in full, is currently being prepared for submission for publication of the material. Bloom, Shelby; Baumann-Pickering, Simone; Rice, Ally; Širović, Ana; Warren, Joseph; Lankhorst, Matthias. The thesis author was the primary investigator and author of this material.

APPENDIX

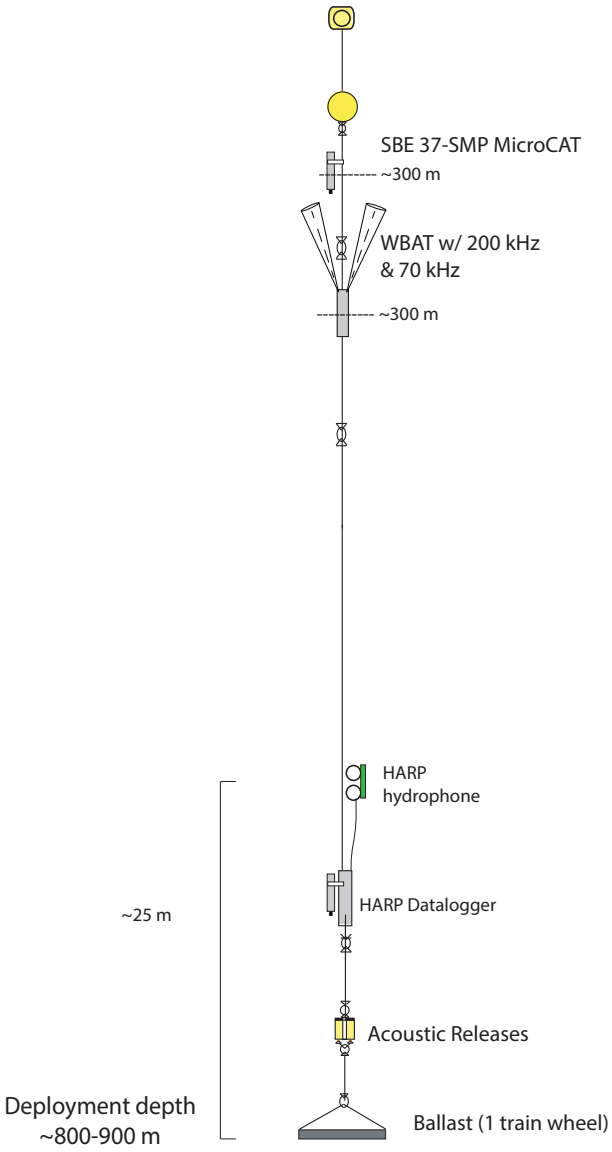

Figure S1: Oceanographic mooring design. Passive acoustic recordings were collected using the high-frequency acoustic recording package (HARP) suspended approximately 25 m above the seafloor. Acoustic backscatter data was collected using the Simrad EK80 Wide Band Autonomous Transceiver (WBAT) located ~300 m from the water surface facing upward. *In situ* water measurements were collected using the autonomous Sea-Bird SBE 37-SMP MicroCAT located ~300 m from the water surface. For deployment 1, two moorings were deployed approximately 1 km apart, with one mooring equipped with the WBAT and ~300 m MicroCAT, and the other with the HARP. For deployments 2 and 3, a single mooring equipped with all 3 instruments was deployed.

Table S1: WBAT-echosounder mission plan parameters for each transducer of each deployment.

Deployment	Transducer Type	Duty Cycle (min)	Number of Active Pings	Number of Passive Pings	Transmitted Pulse Length (ms)	Transmitted Power (W)
1	ES70-18CD (70 kHz)	15	11	4	0.512	150
	ES200-7CD (200 kHz)	15	10	4	0.256	250
2	ES70-18CD (70 kHz)	20	9	4	0.512	150
	ES200-7CD (200 kHz)	20	8	4	0.256	250
3	ES70-18CD (70 kHz)	20	9	4	0.512	150
	ES200-7CD (200 kHz)	20	8	4	0.256	250

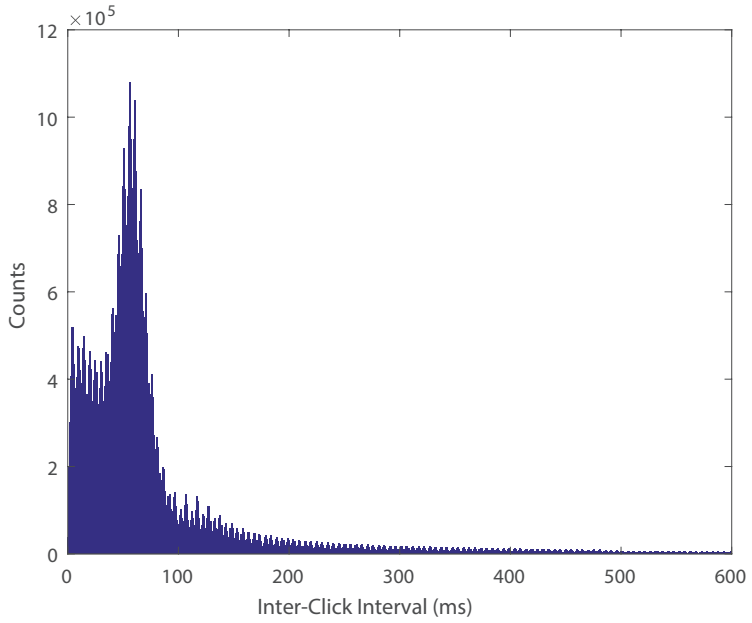

Figure S2: Distribution of inter-click-intervals for common dolphin *Delphinus delphis* echolocation clicks. The observed mode of inter-click-intervals was 56 ms.

Table S2: Blue whale B call automatic detector parameters and outputs for each deployment, with kernel measurements in Table S3.

Deployment	Kernel	Threshold	Precision	Recall
1	1	37	0.968	0.973
2	2	33	0.7713	0.7713
3	3	41	0.7347	0.7616

Table S3: Average extracted frequencies (Hz) at three time points that were used for each kernel listed in Table S2.

Kernel	0 (sec)	1.5 (sec)	3 (sec)	4.5 (sec)	10 (sec)
1	46	45.4	44.7	44.1	43
2	45.9	45.4	44.6	44.1	43.4
3	45.3	45	44.3	43.8	43

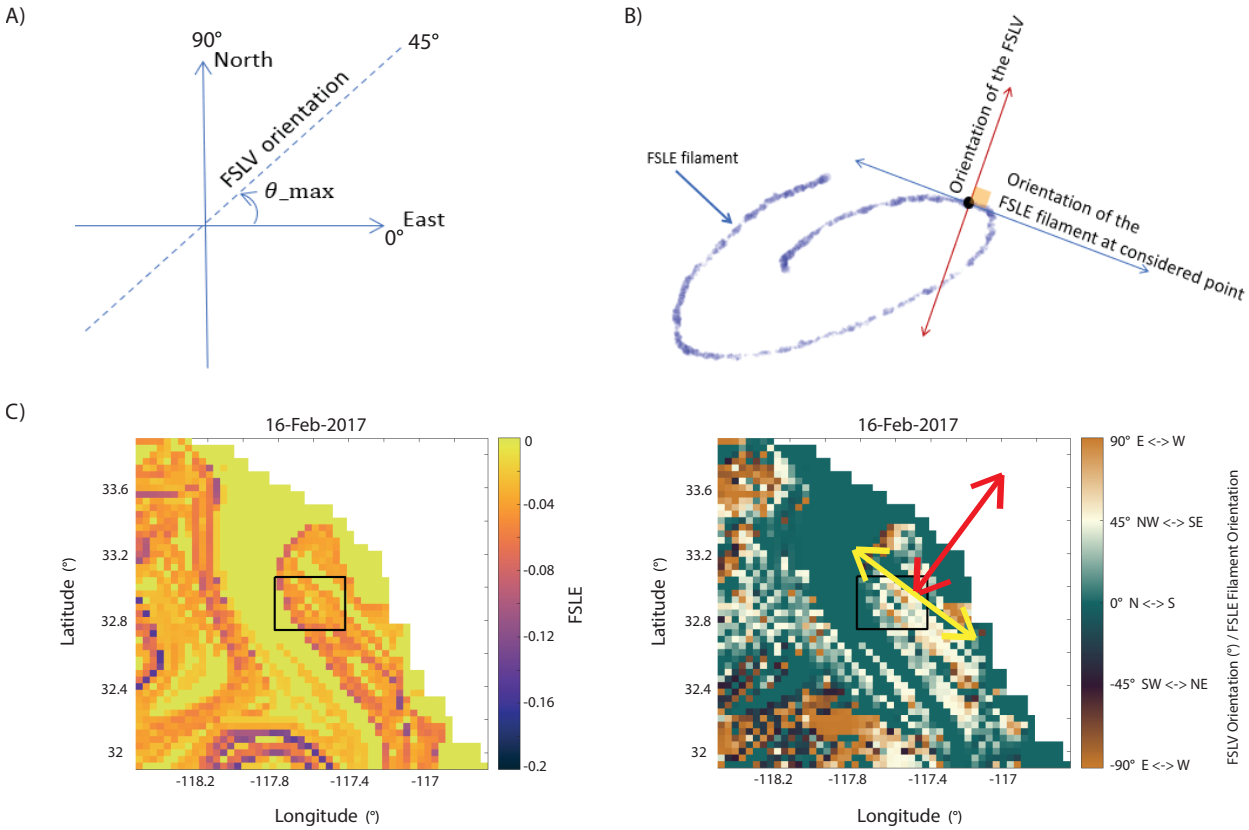

Figure S3: Description of FSLV orientation and FSLE filament orientation. (A) Illustration demonstrating FSLV orientation, which is given as the anticlockwise orientation in degrees of the FSLV with respect to the East direction. FSLV orientation is measured between +/- 90°, where +90° is a N ↔ S orientation, +45° is a SW ↔ NE orientation, 0° is a E ↔ W orientation, -45° is a NW ↔ SE orientation, and -90° is a N ↔ S orientation. (B) Illustration demonstrating that the FSLV is oriented according to the normal of the FSLE filament tangent. As such, the orientation of the FSLE filament based on FSLV orientation is as follows: +90° is a E ↔ W orientation, +45° is a NW ↔ SE orientation, 0° is a N ↔ S orientation, -45° is a SW ↔ NE orientation, and -90° is a E ↔ W orientation. (C) Plots of FSLE and FSLV orientations on February 16, 2017. Black box represents the 20x20 km area around Site T over which environmental variables were averaged. FSLE: darker colors represent more negative FSLE values, hence stronger convergence zone. FSLV: color bar represents the FSLV orientation in degrees, with FSLE filament orientation given as compass orientation. In the FSLV plot, you can see that majority of the FSLE filaments in the black box are +45°, meaning that the associated FSLVs are oriented SW ↔ NE (represented by red arrows); hence the FSLE filaments are normally oriented NW ↔ SE (represented by yellow arrows).

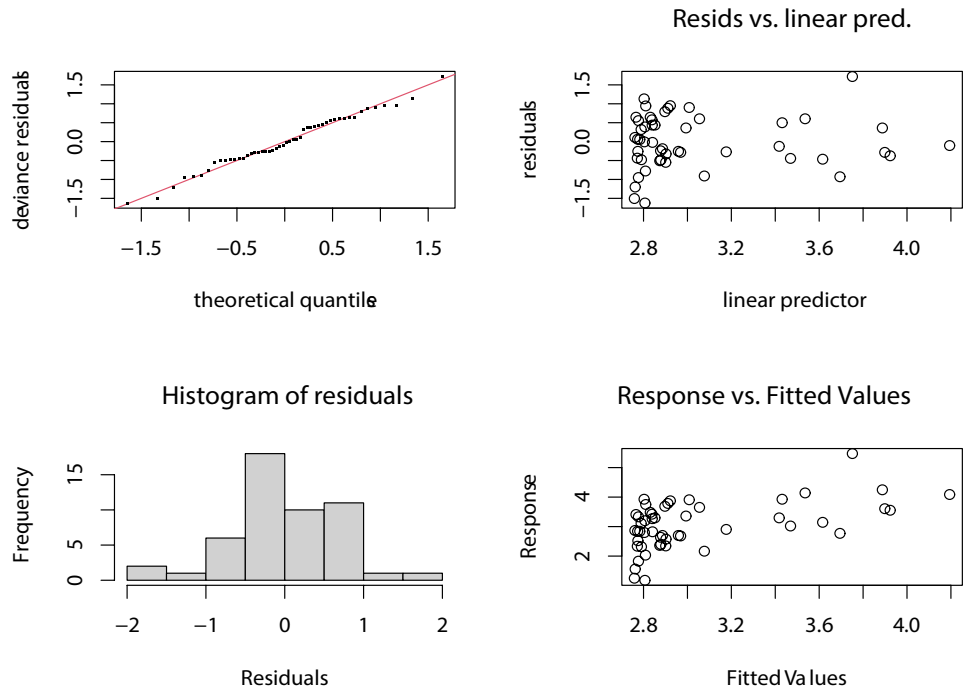

Figure S4: GAM check plots for 70 kHz NASC between 5-50 m.

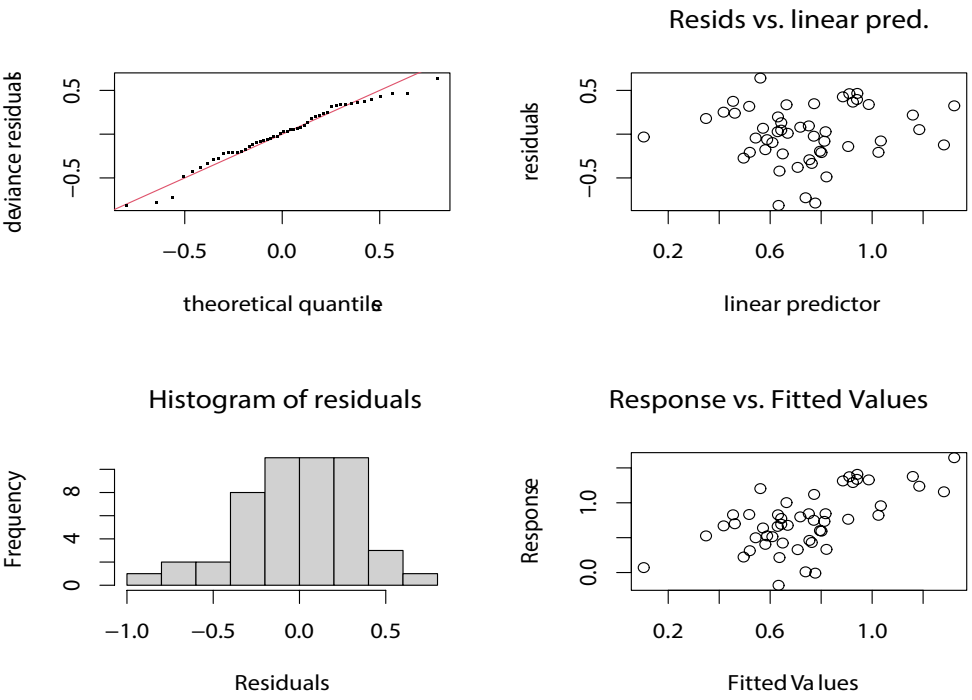

Figure S5: GAM check plots for 70 kHz NASC between 100-150 m.

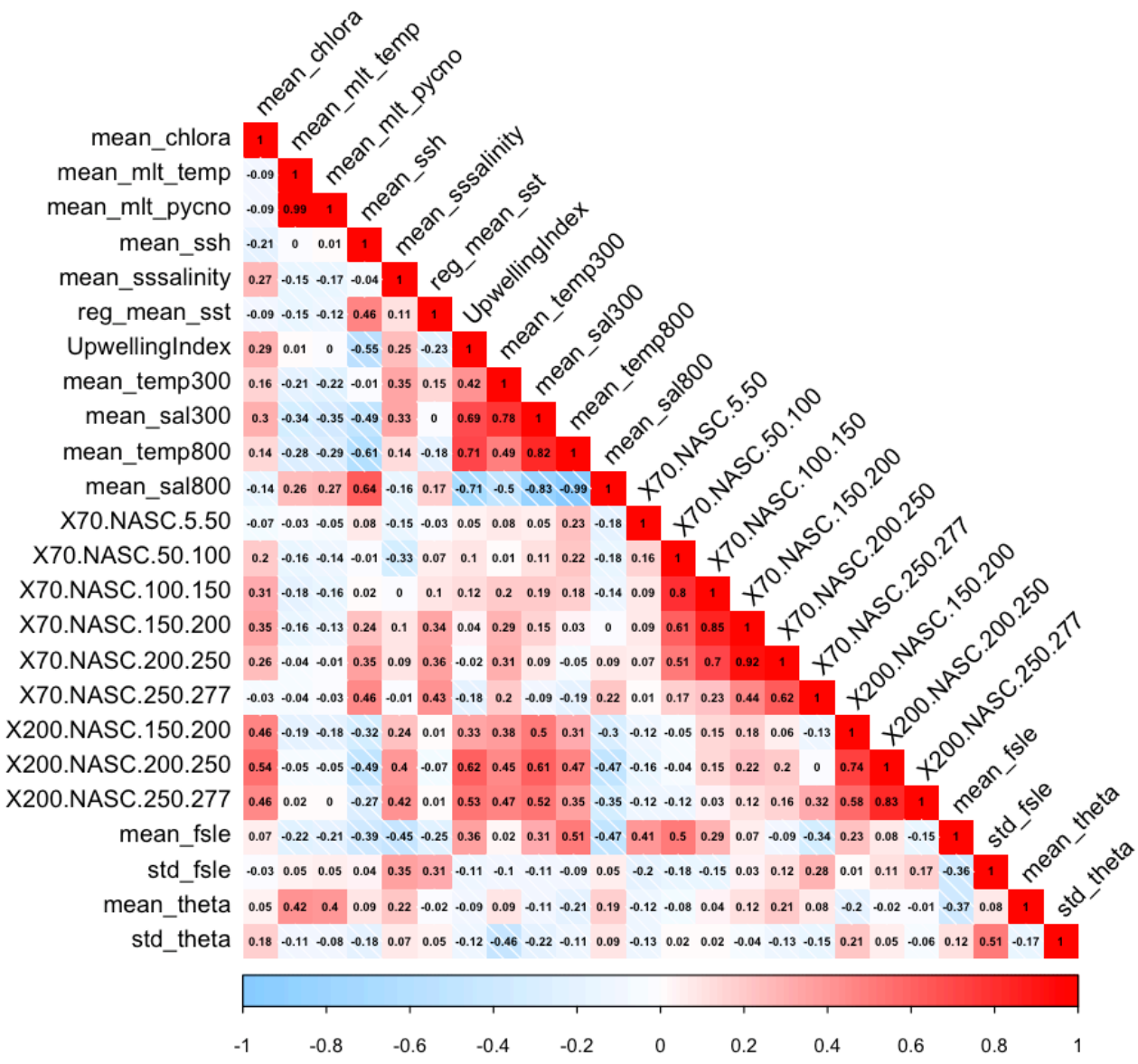

Figure S6: Correlation matrix of variables used in common dolphin GAM model.

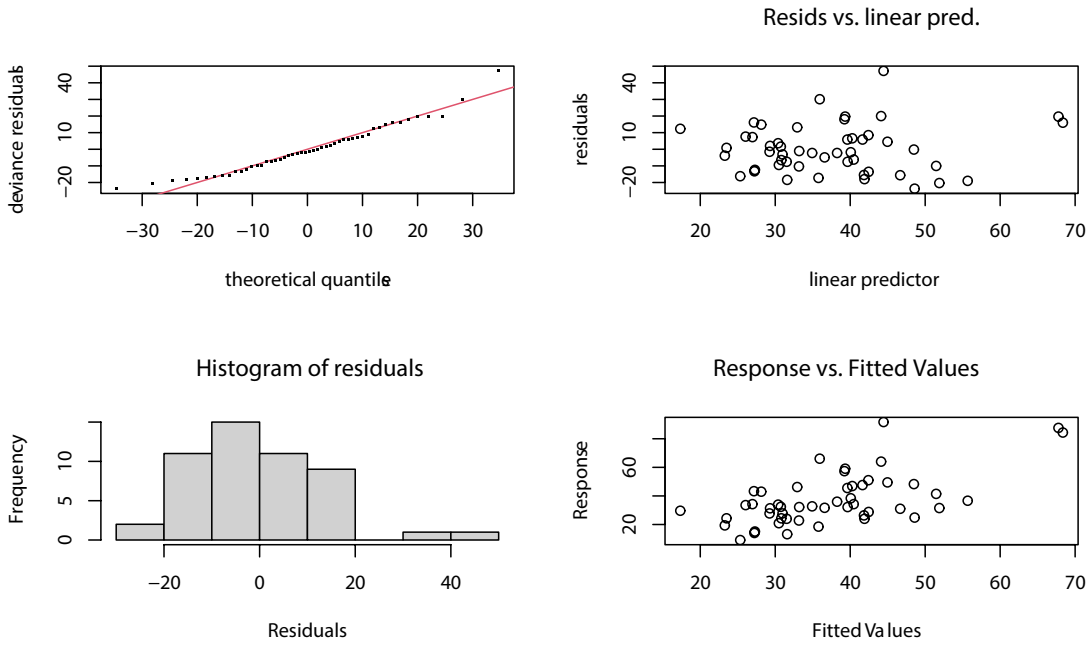

Figure S7: GAM check plots for common dolphin *Delphinus delphis*.

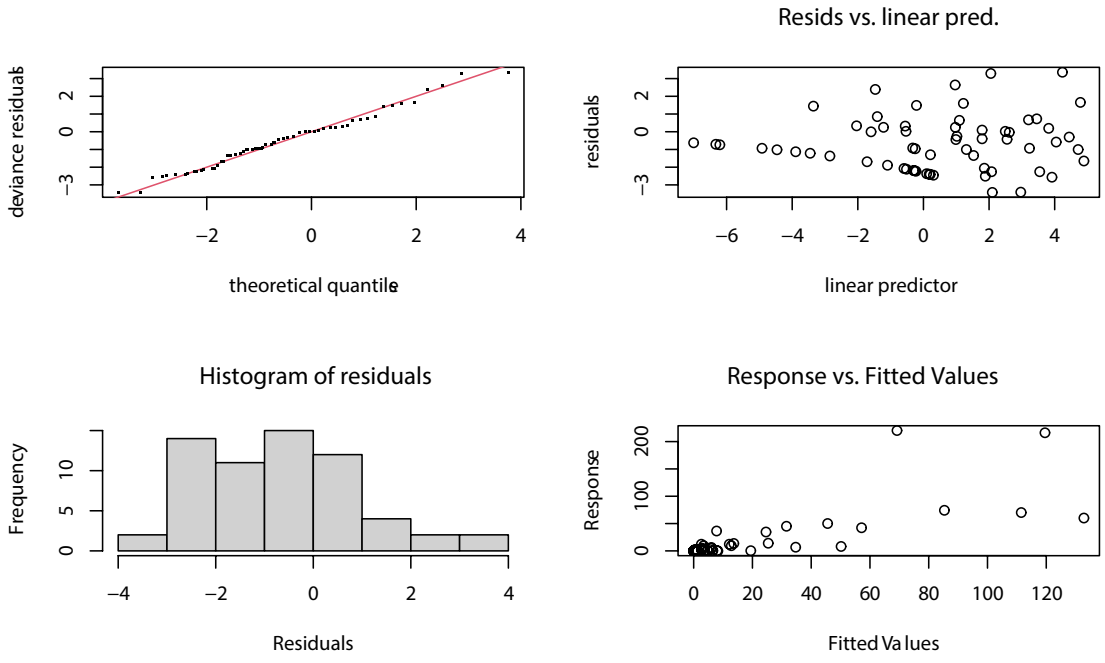

Figure S8: GAM check plots for blue whale *Balaenoptera musculus* D calls.

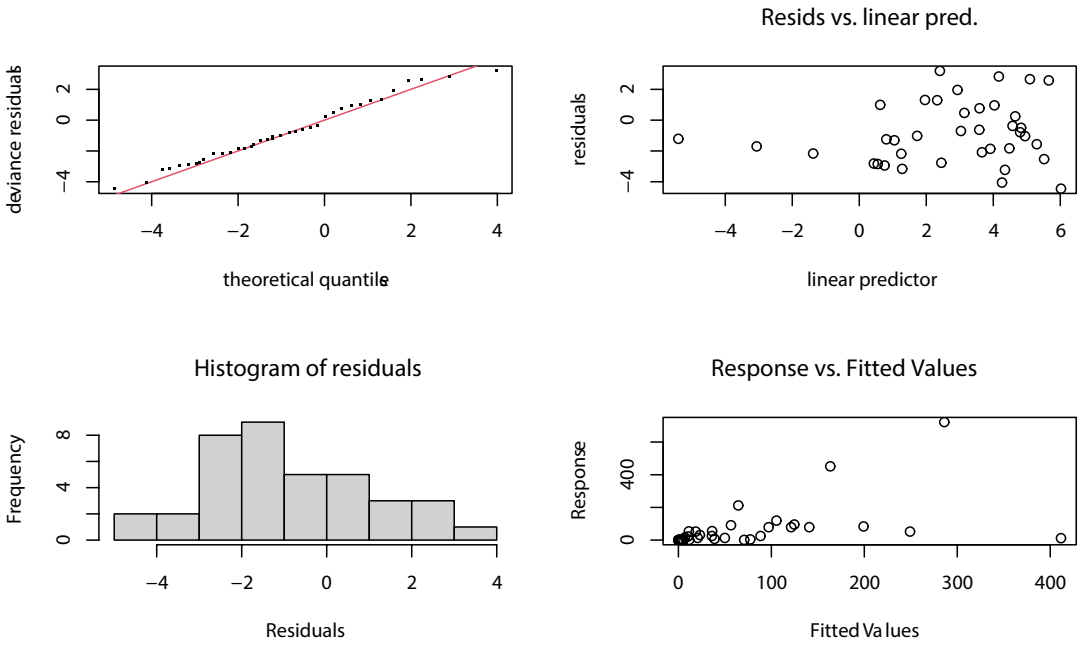

Figure S9: GAM check plots for blue whale *Balaenoptera musculus* B calls.

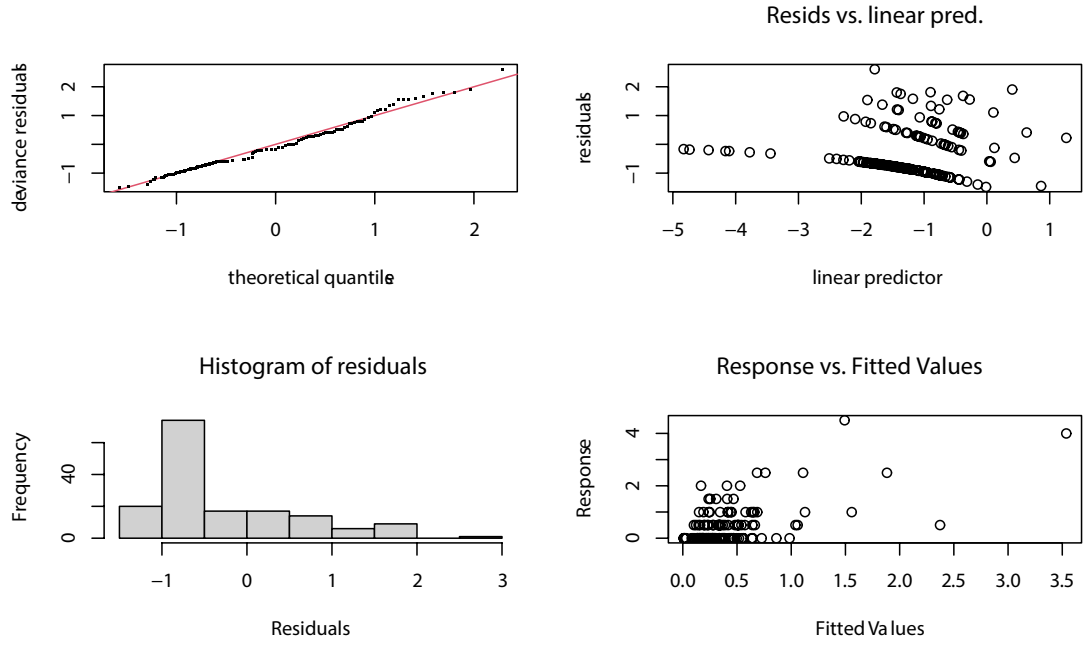

Figure S10: GAM check plots for fin whale *Balaenoptera physalus* 40 Hz calls.

REFERENCES

Alksne MN, Kok ACM, Frasier KE, Wiggins SM, Baumann-Pickering S (in prep.) Using a deep neural network to classify echolocation clicks and identify spatio-temporal patterns of Pacific white-sided dolphins.

Au WWL, Hastings MC (2008) Principles of marine bioacoustics. Springer US, New York, NY

Bakun A (1973) Coastal upwelling indices, west coast of North America, 1946-71. NOAA Technical Report NMFS SSRF-671. U.S. Department of Commerce, Seattle, WA

Bakun A (1975) Daily and weekly upwelling indices, west coast of North America, 1967-73. NOAA Technical Report NMSF SSRF-693. U.S. Department of Commerce, Seattle, WA

Barlow J, Forney KA (2007) Abundance and population density of cetaceans in the California Current ecosystem. Fishery Bulletin 105:509-526

Baumann-Pickering S, McDonald MA, Simonis AE, Solsona Berga A, Merkens KPB, Oleson EM, Roch MA, Wiggins SM, Rankin S, Yack TM, Hildebrand JA (2013) Species-specific beaked whale echolocation signals. The Journal of the Acoustical Society of America 134:2293-2301

Baumann-Pickering S, Roch MA, Brownell JRL, Simonis AE, McDonald MA, Solsona-Berga A, Oleson EM, Wiggins SM, Hildebrand JA (2014) Spatio-temporal patterns of beaked whale echolocation signals in the North Pacific. PLOS ONE 9:e86072

Bialonski S, Caron DA, Schloen J, Feudel U, Kantz H, Moorthi SD (2016) Phytoplankton dynamics in the Southern California Bight indicate a complex mixture of transport and biology. Journal of Plankton Research 38:1077-1091

Buchan SJ, Pérez-Santos I, Narváez D, Castro L, Stafford KM, Baumgartner MF, Valle-Levinson A, Montero P, Gutiérrez L, Rojas C, Daneri G, Neira S (2021) Intraseasonal variation in southeast Pacific blue whale acoustic presence, zooplankton backscatter, and oceanographic variables on a feeding ground in Northern Chilean Patagonia. Progress in Oceanography 199:102709

Checkley DM, Barth JA (2009) Patterns and processes in the California Current System. Progress in Oceanography 83:49-64

Chen CT, Millero FJ (1977) Speed of sound in seawater at high pressures. The Journal of the Acoustical Society of America on CD-ROM 62:1129-1135

Cimino MA, Santora JA, Schroeder I, Sydeman W, Jacox MG, Hazen EL, Bograd SJ (2020) Essential krill species habitat resolved by seasonal upwelling and ocean circulation models within the large marine ecosystem of the California Current System. Ecography 43:1536-1549

Crane NL, Lashkari K (1996) Sound production of gray whales, *Eschrichtius robustus*, along their migration route: A new approach to signal analysis. The Journal of the Acoustical Society of America 100:1878-1886

Croll DA, Marinovic B, Benson S, Chavez FP, Black N, Ternullo R, Tershy BR (2005) From wind to whales: Trophic links in a coastal upwelling system. Marine Ecology Progress Series 289:117-130

d'Ovidio F, De Monte S, Alvain S, Dandonneau Y, Levy M (2010) Fluid dynamical niches of phytoplankton types. Proceedings of the National Academy of Sciences 107:18366-18370

d'Ovidio F, Fernandez V, Hernandez-Garcia E, Lopez C (2004) Mixing structures in the Mediterranean Sea from finite-size Lyapunov exponents. Geophysical Research Letters 31:L17203

Davison PC, Checkley DM, Koslow JA, Barlow J (2013) Carbon export mediated by mesopelagic fishes in the northeast Pacific Ocean. Progress in Oceanography 116:14-30

Demer DA, Berger L, Bernasconi M, Bethke E, Boswell K, Chu D, Domokos R, Dunford A, Fassler S, Gauthier S, Hufnagle LT, Jech JM, Bouffant N, Lebourges-Dhaussy A, Lurton X, Macaulay GJ, Perrot Y, Ryan T, Parker-Stetter S, Stienessen S, Weber T, Williamson N (2015) Calibration of acoustic instruments. ICES Cooperative Research Report No. 326

Douglas AB, Calambokidis J, Munger LM, Soldevilla MS, Ferguson MC, Havron AM, Camacho DL, Campbell GS, Hildebrand JA (2014) Seasonal distribution and abundance of cetaceans off southern California estimated from CalCOFI cruise data from 2004 to 2008. Fishery Bulletin 112:198-220

Eckman JE, Thistle D (1991) Effects of flow about a biologically produced structure on harpacticoid copepods in San Diego Trough. Deep-Sea Research Part A 38:1397-1416

Falkowski PG, Ziemann D, Kolber Z, Bienfang PK (1991) Role of eddy pumping in enhancing primary production in the ocean. Nature 352:55-58

Frasier KE (2021) A machine learning pipeline for classification of cetacean echolocation clicks in large underwater acoustic datasets. PLOS Computational Biology 17:e1009613

Frasier KE, Roch MA, Soldevilla MS, Wiggins SM, Garrison LP, Hildebrand JA (2017) Automated classification of dolphin echolocation click types from the Gulf of Mexico. PLOS Computational Biology 13:e1005823

Frederiksen M, Edwards M, Richardson AJ, Halliday NC, Wanless S (2006) From plankton to top predators: Bottom-up control of a marine food web across four trophic levels. The Journal of Animal Ecology 75:1259-1268

Gaichas S, Skaret G, Falk-Petersen J, Link JS, Overholtz W, Megrey BA, Gjøsæter H, Stockhausen WT, Dommasnes A, Friedland KD, Aydin K (2009) A comparison of community and trophic structure in five marine ecosystems based on energy budgets and system metrics. Progress in Oceanography 81:47-62

Gruber N, Lachkar Z, Frenzel H, Marchesiello P, Münnich M, McWilliams JC, Nagai T, Plattner G-K (2011) Eddy-induced reduction of biological production in eastern boundary upwelling systems. Nature Geoscience 4:787-792

Guiet J, Bianchi D, Maury O, Barrier N, Kessouri F (2022) Movement shapes the structure of fish communities along a cross-shore section in the California Current. Frontiers in Marine Science 9:785282

Helble TA, Ierley GR, D'Spain GL, Roch MA, Hildebrand JA (2012) A generalized power-law detection algorithm for humpback whale vocalizations. The Journal of the Acoustical Society of America 131:2682-2699

Herman LM (2017) The multiple functions of male song within the humpback whale (*Megaptera novaeangliae*) mating system: Review, evaluation, and synthesis. Biological Reviews of the Cambridge Philosophical Society 92:1795-1818

Hickey BM (1979) The California Current System—hypotheses and facts. Progress in Oceanography 8:191-279

Hickey BM (1992) Circulation over the Santa Monica-San Pedro basin and shelf. Progress in Oceanography 30:37-115

Hui CA (1979) Undersea topography and distribution of dolphins of the genus *Delphinus* in the Southern California Bight. Journal of Mammalogy 60:521-527

Irigoien X, Klevjer TA, Røstad A, Martinez U, Boyra G, Acuña JL, Bode A, Echevarria F, Gonzalez-Gordillo JI, Hernandez-Leon S, Agusti S, Aksnes DL, Duarte CM, Kaartvedt S (2014) Large mesopelagic fishes biomass and trophic efficiency in the open ocean. Nature Communications 5:3271

Jory C, Lesage V, Leclerc A, Giard J, Iverson S, Bérubé M, Michaud R, Nozais C (2021) Individual and population dietary specialization decline in fin whales during a period of ecosystem shift. Scientific Reports 11:17181

Lehahn Y, d'Ovidio F, Koren I (2018) A satellite-based Lagrangian view on phytoplankton dynamics. Annual Review of Marine Science 10:99-119

Lewis LA, Calambokidis J, Stimpert AK, Fahlbusch J, Friedlaender AS, McKenna MF, Mesnick SL, Oleson EM, Southall BL, Szesciorka AR, Širović A (2018) Context-dependent variability in blue whale acoustic behaviour. Royal Society Open Science 5:180241

Maclennan DN, Fernandes PG, Dalen J (2002) A consistent approach to definitions and symbols in fisheries acoustics. ICES Journal of Marine Science 59:365-369

McDonald MA, Calambokidis J, Teranishi AM, Hildebrand JA (2001) The acoustic calls of blue whales off California with gender data. The Journal of the Acoustical Society of America 109:1728-1735

McDonald MA, Hildebrand JA, Mesnick S (2009) Worldwide decline in tonal frequencies of blue whale songs. Endangered Species Research 9:13-21

Mellinger DK, Clark CW (2000) Recognizing transient low-frequency whale sounds by spectrogram correlation. The Journal of the Acoustical Society of America 107:3518-3529

Moritz S, Bartz-Beielstein T (2017) imputeTS: Time series missing value imputation in R. The R Journal 9:207

Nieukirk SL, Mellinger DK, Moore SE, Klinck K, Dziak RP, Goslin J (2012) Sounds from airguns and fin whales recorded in the mid-Atlantic Ocean, 1999-2009. The Journal of the Acoustical Society of America 131:1102-1112

Nishimoto MM, Washburn L (2002) Patterns of coastal eddy circulation and abundance of pelagic juvenile fish in the Santa Barbara Channel, California, USA. Marine Ecology Progress Series 241:183-199

Oleson EM, Calambokidis J, Burgess WC, McDonald MA, LeDuc CA, Hildebrand JA (2007) Behavioral context of call production by eastern North Pacific blue whales. Marine Ecology Progress Series 330:269-284

Oschlies A, Garçon V (1998) Eddy-induced enhancement of primary production in a model of the North Atlantic Ocean. Nature 394:266-269

Payne RS, McVay S (1971) Songs of humpback whales. Science 173:585-597

Peacock T, Haller G (2013) Lagrangian coherent structures: The hidden skeleton of fluid flows. Physics Today 66:41-47

Ressler PH, Brodeur RD, Peterson WT, Pierce SD, Mitchell Vance P, Røstad A, Barth JA (2005) The spatial distribution of euphausiid aggregations in the Northern California Current during August 2000. Deep-Sea Research Part II 52:89-108

Rice DW (1965) Offshore southward migration of gray whales off southern California. Journal of Mammalogy 46:504-505

Roch MA, Klinck H, Baumann-Pickering S, Mellinger DK, Qui S, Soldevilla MS, Hildebrand JA (2011) Classification of echolocation clicks from odontocetes in the Southern California Bight. The Journal of the Acoustical Society of America 129:467-475

Romagosa M, Pérez-Jorge S, Cascão I, Mouriño H, Lehodey P, Pereira A, Marques TA, Matias L, Silva MA (2021) Food talk: 40-Hz fin whale calls are associated with prey biomass. Proceedings of the Royal Society B 288:20211156

Rossi V, López C, Hernández-García E, Sudre J, Garçon V, Morel Y (2009) Surface mixing and biological activity in the four Eastern Boundary Upwelling Systems. Nonlinear Processes in Geophysics 16:557-568

Ruzicka JJ, Brink KH, Gifford DJ, Bahr F (2016) A physically coupled end-to-end model platform for coastal ecosystems: Simulating the effects of climate change and changing upwelling characteristics on the Northern California Current ecosystem. Ecological Modelling 331:86-99

Scales KL, Hazen EL, Jacox MG, Castruccio F, Maxwell SM, Lewison RL, Bograd SJ (2018) Fisheries bycatch risk to marine megafauna is intensified in Lagrangian coherent structures. Proceedings of the National Academy of Sciences 115:7362-7367

Scales KL, Schorr GS, Hazen EL, Bograd SJ, Miller PI, Andrews RD, Zerbini AN, Falcone EA, VanDerWal J (2017) Should I stay or should I go? Modelling year-round habitat suitability and drivers of residency for fin whales in the California Current. Diversity & Distributions 23:1204-1215

Selzer LA, Payne PM (1988) The distribution of white-sided (*Lagenorhynchus acutus*) and common dolphins (*Delphinus delphis*) vs. environmental features of the continental shelf of the northeastern United States. Marine Mammal Science 4:141-153

Siegel DA, McGillicuddy DJ, Fields EA (1999) Mesoscale eddies, satellite altimetry, and new production in the Sargasso Sea. Journal of Geophysical Research: Oceans 104:13359-13379

Simonis AE, Roch MA, Bailey B, Barlow J, Clemesha RES, Iacobellis S, Hildebrand JA, Baumann-Pickering S (2017) Lunar cycles affect common dolphin *Delphinus delphis* foraging in the Southern California Bight. Marine Ecology Progress Series 577:221-235

Soldevilla MS, Henderson EE, Campbell GS, Wiggins SM, Hildebrand JA, Roch MA (2008) Classification of Risso's and Pacific white-sided dolphins using spectral properties of echolocation clicks. The Journal of the Acoustical Society of America 124:609-624

Soldevilla MS, Wiggins SM, Hildebrand JA, Oleson EM, Ferguson MC (2011) Risso's and Pacific white-sided dolphin habitat modeling from passive acoustic monitoring. Marine Ecology Progress Series 423:247-260

Solsona-Berga A, Frasier KE, Baumann-Pickering S, Wiggins SM, Hildebrand JA (2020) Detedit: A graphical user interface for annotating and editing events detected in long-term acoustic monitoring data. PLOS Computational Biology 16:e1007598

Stimpert AK, Au WWL, Parks SE, Hurst T, Wiley DN (2011) Common humpback whale (*Megaptera novaeangliae*) sound types for passive acoustic monitoring. The Journal of the Acoustical Society of America 129:476-482

Sumich JL, Show IT (2011) Offshore migratory corridors and aerial photogrammetric body length comparisons of southbound gray whales, *Eschrichtius robustus*, in the Southern California Bight, 1988-1990. Marine Fisheries Review 73:28

Tepsich P, Rosso M, Halpin PN, Moulins A (2014) Habitat preferences of two deep-diving cetacean species in the northern Ligurian Sea. Marine Ecology Progress Series 508:247-260

Titaud O, Brankart J-M, Verron J (2011) On the use of finite-time Lyapunov exponents and vectors for direct assimilation of tracer images into ocean models. Tellus Series A 63:1038-1051

Vu ET, Risch D, Clark CW, Gaylord S, Hatch LT, Thompson MA, Wiley DN, Van Parijs SM (2012) Humpback whale song occurs extensively on feeding grounds in the western North Atlantic Ocean. Aquatic Biology 14:175-183

Wiggins SM, Garsha C, Campbell G, Hildebrand JA (2006) High- frequency Acoustic Recording Package (HARP) for long- term monitoring of marine mammals. The Journal of the Acoustical Society of America 120:3015

Wood SN (2006) Generalized additive models: An introduction with R. Chapman & Hall/CRC, Boca Raton, FL

Young JW, Hunt BPV, Cook TR, Llopiz JK, Hazen EL, Pethybridge HR, Ceccarelli D, Lorrain A, Olson RJ, Allain V, Menkes C, Patterson T, Nicol S, Lehodey P, Kloser RJ, Arrizabalaga H, Anela Choy C (2015) The trophodynamics of marine top predators: Current knowledge, recent advances and challenges. Deep-Sea Research Part II 113:170-187

Zuur AF, Ieno EN, Walker NJ, Saveliev AA, Smith GM (2009) Mixed effects models and extensions in ecology with R. Springer, New York, NY

Širović A (2016) Variability in the performance of the spectrogram correlation detector for North-east Pacific blue whale calls. Bioacoustics 25:145-160

Širović A, Hildebrand JA (2011) Using passive acoustics to model blue whale habitat off the Western Antarctic Peninsula. Deep-Sea Research Part II 58:1719-1728

Širović A, Hildebrand JA, Wiggins SM, McDonald MA, Moore SE, Thiele D (2004) Seasonality of blue and fin whale calls and the influence of sea ice in the Western Antarctic Peninsula. Deep-Sea Research Part II 51:2327-2344

Širović A, Rice A, Chou E, Hildebrand JA, Wiggins SM, Roch MA (2015) Seven years of blue and fin whale call abundance in the Southern California Bight. Endangered Species Research 28:61-76

Širović A, Williams LN, Kerosky SM, Wiggins SM, Hildebrand JA (2012) Temporal separation of two fin whale call types across the eastern North Pacific. Marine Biology 160:47-57